



HAL
open science

Ultra diffuse galaxies in the MATLAS low-to-moderate density fields

Francine Marleau, Rebecca Habas, Mélina Poulain, Pierre-Alain Duc, Oliver Müller, Sungsoon Lim, Patrick Durrell, Rubén Sánchez-Janssen, Sanjaya Paudel, Syeda Lammim Ahad, et al.

► **To cite this version:**

Francine Marleau, Rebecca Habas, Mélina Poulain, Pierre-Alain Duc, Oliver Müller, et al.. Ultra diffuse galaxies in the MATLAS low-to-moderate density fields. *Astronomy and Astrophysics - A&A*, 2021, 654, pp.A105. 10.1051/0004-6361/202141432 . hal-03413315

HAL Id: hal-03413315

<https://hal.science/hal-03413315v1>

Submitted on 17 Jun 2022

HAL is a multi-disciplinary open access archive for the deposit and dissemination of scientific research documents, whether they are published or not. The documents may come from teaching and research institutions in France or abroad, or from public or private research centers.

L'archive ouverte pluridisciplinaire **HAL**, est destinée au dépôt et à la diffusion de documents scientifiques de niveau recherche, publiés ou non, émanant des établissements d'enseignement et de recherche français ou étrangers, des laboratoires publics ou privés.

Ultra diffuse galaxies in the MATLAS low-to-moderate density fields[★]

Francine R. Marleau¹, Rebecca Habas², Mélina Poulain¹, Pierre-Alain Duc², Oliver Müller², Sungsoon Lim³, Patrick R. Durrell⁴, Rubén Sánchez-Janssen⁵, Sanjaya Paudel³, Syeda Lammim Ahad⁶, Abhishek Chougule^{7,8}, Michal Bílek⁹, and Jérémy Fensch¹⁰

¹ Institut für Astro- und Teilchenphysik, Universität Innsbruck, Technikerstraße 25/8, Innsbruck 6020, Austria
e-mail: francine.marleau@uibk.ac.at

² Observatoire Astronomique de Strasbourg (ObAS), Université de Strasbourg – CNRS, UMR 7550, Strasbourg, France

³ Department of Astronomy, Yonsei University, 50 Yonsei-ro Seodaemun-gu, Seoul 03722, Republic of Korea

⁴ Youngstown State University, One University Plaza, Youngstown, OH 44555, USA

⁵ UK Astronomy Technology Centre, Royal Observatory, Blackford Hill, Edinburgh EH9 3HJ, UK

⁶ Leiden Observatory, Leiden University, PO Box 9513, 2300 RA Leiden, The Netherlands

⁷ Instituto de Astrofísica e Ciências do Espaço, Universidade do Porto, CAUP, Rua das Estrelas, 4150-762 Porto, Portugal

⁸ Departamento de Física e Astronomia, Faculdade de Ciências, Universidade do Porto, Rua do Campo Alegre 687, 4169-007 Porto, Portugal

⁹ Nicolaus Copernicus Astronomical Center, Polish Academy of Sciences, Bartycka 18, 00-716 Warsaw, Poland

¹⁰ Univ. Lyon, ENS de Lyon, Univ. Lyon 1, CNRS, Centre de Recherche Astrophysique de Lyon, UMR5574, 69007 Lyon, France

Received 31 May 2021 / Accepted 14 September 2021

ABSTRACT

Recent advances in deep dedicated imaging surveys over the past decade have uncovered a surprisingly large number of extremely faint low surface brightness galaxies with large physical sizes called ultra diffuse galaxies (UDGs) in clusters and, more recently, in lower density environments. As part of the Mass Assembly of early-Type GaLaxies with their fine Structures (MATLAS) survey, a deep imaging large program at the Canada-France-Hawaii Telescope (CFHT), our team has identified 2210 dwarf galaxies, 59 (~3%) of which qualify as UDGs. Averaging over the survey area, we find ~0.4 UDG per square degree. They are found in a range of low to moderate density environments, although 61% of the sample fall within the virial radii of groups. Based on a detailed analysis of their photometric and structural properties, we find that the MATLAS UDGs do not show significant differences from the traditional dwarfs, except from the predefined size and surface brightness cut. Their median color is as red as the one measured in galaxy clusters, albeit with a narrower color range. The majority of the UDGs are visually classified as dwarf ellipticals with log stellar masses of ~6.5–8.7. The fraction of nucleated UDGs (~34%) is roughly the same as the nucleated fraction of the traditional dwarfs. Only five (~8%) UDGs show signs of tidal disruption and only two are tidal dwarf galaxy candidates. A study of globular cluster (GC) candidates selected in the CFHT images finds no evidence of a higher GC specific frequency S_N for UDGs than for classical dwarfs, contrary to what is found in most clusters. The UDG halo-to-stellar mass ratio distribution, as estimated from the GC counts, peaks at roughly the same value as for the traditional dwarfs, but spans the smaller range of ~10–2000. We interpret these results to mean that the large majority of the field-to-group UDGs do not have a different formation scenario than traditional dwarfs.

Key words. Galaxy: general – galaxies: formation – galaxies: dwarf – galaxies: fundamental parameters – galaxies: nuclei – galaxies: star clusters: general

1. Introduction

Recent advances in deep dedicated imaging surveys over the past decade have uncovered a surprisingly large number of extremely faint low surface brightness (LSB) galaxies with large physical sizes referred to as ultra diffuse galaxies (UDGs). Although the name was branded recently (van Dokkum et al. 2015), large LSB galaxies have been observed over three decades (e.g., Sandage & Binggeli 1984; Binggeli et al. 1985; Impey et al. 1988; Schombert & Bothun 1988; Schwartzberg et al. 1995; Dalcanton et al. 1997; Sprayberry et al. 1997). UDGs are defined as having a low central surface brightness, with typical values in the g -band on the order of $\mu_{0,g} = 24\text{--}26$ mag arcsec⁻²,

but unlike the ultra faint dwarf galaxies, they have a large physical size, with effective radii $R_e > 1.5$ kpc (van Dokkum et al. 2015). Andromeda XIX, a satellite of M31, is an example of a Local Group (LG) UDG with a half-light radius of 1.7 kpc (McConnachie et al. 2008).

Almost all UDGs discovered until recently resided in dense cluster environments, including the central regions (Koda et al. 2015) and outskirts (Kadowaki et al. 2017; van Dokkum et al. 2015) of the Coma cluster, the Fornax cluster (Muñoz et al. 2015; Venhola et al. 2017), and other clusters (e.g., Mihos et al. 2015; van der Burg et al. 2016; Román & Trujillo 2017a). At the distance of their respective clusters, their estimated physical sizes are $1.5 < R_e < 4.6$ kpc, with the largest ones rivaling the size of the Milky Way ($R_{e,MW} \sim 3.6$ kpc). For comparison, the typical dwarf galaxies in the same luminosity range have effective radii of a few hundred parsecs (Müller et al. 2019;

[★] Data are also available at the CDS via anonymous ftp to cdsarc.u-strasbg.fr (130.79.128.5) or via <http://cdsarc.u-strasbg.fr/viz-bin/cat/J/A+A/654/A105>

Chiboucas et al. 2013). Observations indicate that the UDGs found in rich galaxy clusters (van Dokkum et al. 2015; Gu et al. 2018) are typically old, red ($g - i \sim 0.76$), gas and metal poor, relatively round and featureless, although not all cluster UDGs are devoid of gas and sources of ionizing radiation (e.g., Kadowaki et al. 2017). Based on their globular cluster (GC) population, they have a wide range of physical properties with many showing low-mass (dwarf) haloes. However, the most discussed cases have been the “dark matter deficient” (NGC 1052-DF2 and NGC 1052-DF4, van Dokkum et al. 2018a,b, 2019; Emselem et al. 2019; Fensch et al. 2019b) and “massive Milky Way like” UDGs (Dragonfly 44, van Dokkum et al. 2016; Beasley et al. 2016; Toloba et al. 2018) that do not follow the stellar mass-halo mass relationship predicted by the Λ cold dark matter (ACDM) cosmological model (Behroozi et al. 2013). A recent report of the lack of X-ray detection suggests that Dragonfly 44 and DF X1 are not failed L_* galaxies (Bogdán 2020).

The GCs themselves in some UDGs also appear to be too luminous, with them being as bright or brighter than Omega Centauri (van Dokkum et al. 2018a; Shen et al. 2021). The recent analysis of the GC population in the UDG MATLAS-2019, in the NGC 5846 group, using deep – sampling most of the globular cluster luminosity function (GCLF) – high resolution *Hubble* Space Telescope (HST) data (Müller et al. 2021) has revealed that the brightest GCs in this UDG are consistent with the normal bright end of the GCLF at the group distance, indicating there are no over-luminous GCs present in this galaxy, contrary to what is found for NGC 1052-DF2 and -DF4 (Danieli et al. 2019; Shen et al. 2021). Rather, the GCLF is best explained by a large population of GCs for a galaxy of this luminosity. Recent results for 33 UDGs in the Coma cluster based on HST observations similarly suggest that UDGs can reach a high specific frequency ($0 < S_N < 50$, Lim et al. 2018), with a mean S_N higher for UDGs than for classical dwarfs. In this cluster, Forbes et al. (2020) find that the rich GC systems tend to be hosted in UDGs of a lower luminosity, smaller size, and fainter surface brightness, with a similar trend for the normal dwarfs. The GC systems of Virgo UDGs have a wide range in specific frequency, with a higher mean S_N than normal Virgo dwarfs, but a lower mean S_N than Coma UDGs at a fixed luminosity (Lim et al. 2020). In the Fornax cluster, Prole et al. (2019a) find very few UDGs with a high S_N . Rather their GC numbers are consistent with those of other dwarf galaxies of a comparable luminosity. The different abundances of GCs, especially the demarcation between UDGs with and without an excess of GCs as compared to the normal dwarfs, may point to different origins.

Recently, a growing number of UDGs have been identified in nearby groups using blind optical surveys (Merritt et al. 2016; Bennet et al. 2017 in the M101 group with the Dragonfly Telescope Array and as part of the Canada-France-Hawaii Telescope Legacy Survey (CFHTLS), Román & Trujillo 2017b in the Sloan Digital Sky Survey (SDSS) Stripe 82, Greco et al. 2018 in the Hyper Suprime-Cam Subaru Strategic Program (HSC-SSP), Forbes et al. 2019, 2020 in the VST Early-type GALaxy Survey (VEGAS)) and blind HI surveys (Du et al. 2015 using ALFALFA+SDSS, Leisman et al. 2017 using ALFALFA+SDSS,WIYN), as well as in low density environments such as the Pisces-Perseus supercluster (DGSAT I, Martínez-Delgado et al. 2016), the MATLAS (Mass Assembly of early-Type GaLaxies with their fine Structures) survey (Habas et al. 2020), the SDSS Stripe 82 (Barbosa et al. 2020) and other isolated spiral and early-type spiral galaxies (Román et al. 2019; Müller et al. 2018a; For et al. 2019; Crnojević et al. 2014). The UDGs found in groups are typically

blue ($g - i \sim 0.45$) and irregular (Román & Trujillo 2017b). The UDGs found in the low to moderate density environments of the MATLAS survey (Habas et al. 2020) do not appear to form a distinct group in the scaling relations but are simply an extension of the dwarf population toward larger radii and fainter surface brightnesses. X-Ray observations of multiple UDGs (Kovács et al. 2019) also support the fact that the majority of UDGs are consistent with being normal dwarfs even though this does not exclude the possibility that some UDGs may have been failed Milky Way galaxies. The field UDG candidates of Barbosa et al. (2020) – as they have no distance estimates so are given a redshift by association to the nearby overdensity of normal galaxies – appear to have stellar masses and metallicities that are similar to those observed in clusters. Other works on field UDGs have shown that they can contain HI gas (Poulain et al. 2021b; Leisman et al. 2017) and are predominantly blue and star forming (Prole et al. 2019b).

Various scenarios have been put forward to explain the formation of UDGs, based on the properties of the population of UDGs in galaxy clusters. It may be that they are “failed” high halo mass galaxies, prevented from building a normal stellar population due to, for example, extreme feedback from supernovae and young stars, gas stripping, or AGN feedback. On the other hand, UDGs may be “genuine” dwarf galaxies with correspondingly low halo masses but anomalously large sizes. They could represent the most rapidly spinning tail of the distribution of dwarf galaxies (Amorisco & Loeb 2016), or feedback and outflow could create an expansion of both the dark matter and stellar component of dwarf galaxies (Di Cintio et al. 2017). Several UDGs show highly elongated shapes, suggestive of tidal disruption (Merritt et al. 2016; Mihos et al. 2015). Another scenario is that some UDGs could be tidal dwarf galaxies (TDGs), that is galaxies formed from gas expelled from a massive galaxy after an interaction. TDGs are known to be devoid of dark matter (Lelli et al. 2015), have a higher metallicity and radius than dwarfs of similar mass (Weilbacher et al. 2003; Duc et al. 2014) and their GCs are less massive (Fensch et al. 2019a). The old ones have the same properties as UDGs (Duc et al. 2014).

A recent survey for dwarf galaxies in the MATLAS low to medium density fields has revealed 2210 low surface brightness galaxies (Habas et al. 2020). In this paper, we identify the UDGs in the MATLAS sample and present their detailed properties. In Sect. 2 we discuss the observations and data analysis of the MATLAS sample as well as the UDG selection procedure. In Sect. 4, we examine the types of environments in which the MATLAS UDGs are located. The photometric and structural properties of the UDG, as well as their compact central nuclei when present, are presented in Sect. 5. Their derived stellar masses are also discussed in this section. In Sect. 6, we determine the globular cluster populations of the UDGs and compute their estimated halo masses. We search for possible tidal features and present the results in Sect. 7. The UDGs with HI detections are discussed in Sect. 8. Finally, in Sect. 9, we summarize our results.

2. MATLAS dwarf galaxy sample

2.1. Observations and catalog

The UDG candidates were identified from the deep ($\mu_g \sim 28.5\text{--}29$ mag arcsec⁻²) optical imaging of the Mass Assembly of early-Type gaLaxies with their fine Structures (MATLAS) large observing program (Duc et al. 2014, 2015; Duc 2020; Bílek et al. 2020). MATLAS was designed to study the

low surface brightness outskirts of massive early-type galaxies (ETGs) in low- and moderate- density environments in the nearby ($z < 0.01$) Universe. The target galaxies were taken from the ATLAS^{3D} legacy survey (Cappellari et al. 2011a), which compiled a complete sample of galaxies (the “parent” sample) with distances between ≈ 10 –45 Mpc, declinations obeying $|\delta - 29^\circ| < 35^\circ$, Galactic latitudes $|b| > 15^\circ$, and K -band absolute magnitudes $M_K < -21.5$. The galaxies were morphologically reclassified by the ATLAS^{3D} team for consistency, and only the 260 elliptical and lenticular galaxies were included in the final sample. The Next Generation Virgo Cluster Survey (NGVS; Ferrarese et al. 2012) survey obtained deep optical imaging of the 58 ATLAS^{3D} ETGs within the virial radius of the Virgo cluster, while MATLAS planned to target the remaining (non-Virgo) ETGs.

The MATLAS (and NGVS) images were taken with MegaCam on the 3.6 meter Canada-France-Hawaii Telescope (CFHT). MATLAS ultimately imaged $150 1^\circ \times 1^\circ$ fields, encompassing 180 ETGs and 59 late-type galaxies (LTGs), with an ETG typically at (or very near) the center of the image. This field of view corresponds to physical scales ranging from approximately 175 kpc ($d = 10$ Mpc) to 785 kpc ($d = 45$ Mpc). Select fields in moderate density environments have some overlap, however, thus the total coverage of the survey is 142 square degrees. The fields were preferentially observed first in the g -band (150 fields), followed by the r -band (148 fields), the i -band (77 fields), and the nearest fields ($d_{\text{ETG}} < 20$ Mpc) in the u -band (12 fields). All magnitudes presented in this paper were calibrated in the MegaCam AB magnitude system. Details of the observing strategy, data reduction, and image quality can be found in Duc et al. (2015), while a full list of targeted fields is presented in Table 1 of Habas et al. (2020), and Bílek et al. (2020) presents a comparison with other recent deep imaging surveys.

The depth and image quality of the MATLAS survey is ideal for identifying new low surface brightness galaxies. The systematic search for dwarfs in the MATLAS images is described in detail in Habas et al. (2020), but we briefly outline the selection criteria here for completeness. We first compiled a catalog of dwarf candidates from a visual inspection of every MATLAS image; this was then used to test various SExtractor (Bertin & Arnouts 1996) detection parameters, which were tweaked until $\sim 90\%$ of the visually identified dwarfs were successfully extracted. The visual catalog was then supplemented with additional candidates from SExtractor, identified by their surface brightness μ_g , g -band magnitude, and size. This joint catalog underwent two rounds of visual classification and cleaning, resulting in the final catalog of 2210 dwarfs based on the majority opinion of the final five classifiers. Further details, comparisons with overlapping catalogs, and discussions of the limitations and biases of the catalog can be found in Habas et al. (2020).

2.2. MATLAS dwarf distances

Distances are essential to characterise many properties of dwarf galaxies, for example, absolute magnitudes, effective radii in physical units, and determining the local environment of the dwarf. We have distance estimates for a fraction (14.7%; 325) of the MATLAS dwarfs from various sources: spectroscopic redshifts from SDSS DR13 (Blanton et al. 2017; Albareti et al. 2017) and the Catalog of Visually Classified Galaxies (CVCG; Ann et al. 2015), HI velocities from the ALFALFA catalog (Haynes et al. 2018) and the Westerbork Synthesis Radio Telescope (WSRT) imaging data of the ATLAS^{3D} targets (Serra et al.

2012; Poulain et al. 2021a), distances from the NEARGALCAT (Karachentsev et al. 2013), as well as stacked MUSE spectra and a distance estimate from the GCLF for MATLAS-2019 (Müller et al. 2020, 2021).

Previous work has demonstrated that these galaxies are all dwarf-like systems with absolute magnitudes $M_g \geq -18$ and that $>90\%$ of them are satellites of the nearest massive galaxy in the ATLAS^{3D} parent (ETG + LTG) sample with relative velocities $|\Delta v| < 500 \text{ km s}^{-1}$ (Habas et al. 2020; Poulain et al. 2021b). It should be noted that 21 (6%) of these galaxies, however, have distance estimates >45 Mpc, so we would not expect to find a good host among the massive ATLAS^{3D} galaxies. This further strengthens the argument that the dwarfs in our sample are overwhelmingly expected to be satellite galaxies. Thus, if we can identify the likely host of the dwarfs without known distances, we are able to use the distance of the host as the distance for these dwarf with some degree of confidence. Habas et al. (2020) used the subsample of dwarfs with known distances to test the accuracy of the host identification using other methods – by assuming either the MATLAS targeted ETG (often the most massive and most central ETG in the image) is the host, or that the ATLAS^{3D} massive galaxy (ETG or LTG) with the smallest on-sky separation is the host. The accuracy of both tests was $\sim 80\%$.

We opted to proceed under the assumption that all of the dwarfs are satellites of a massive galaxy, and adopted the distance of the MATLAS targeted ETG when no other distance estimates are available.

2.3. MATLAS dwarf structural parameters

The structural and photometric properties of each MATLAS dwarf galaxy were extracted using GALFIT (Peng et al. 2002, 2010). The nonnucleated dwarfs were fitted with a single Sérsic profile in the g , r and i bands, measuring their effective radius (R_e), Sérsic index (n), total magnitude, and axis ratio. The g -band surface brightnesses $\mu_{0,g}$ (central), $\mu_{e,g}$ (at R_e) and $\langle \mu_{e,g} \rangle$ (within R_e) were then calculated using the equations in Graham & Driver (2005) taking as inputs the total magnitude and effective radius returned by GALFIT. The galaxy model $g - i$ and $g - r$ colors were computed when images were available in these bands (see Sect. 2.1). When hosting one or multiple nuclei, the galaxies were fitted instead with a Sérsic profile (for the galaxy) and a PSF/King profile (for each nucleus) simultaneously. For nucleated galaxies, the properties reported for the dwarf relate to the galaxy (Sérsic profile). The detailed properties of the nucleus/nuclei are discussed in Sect. 5. The GALFIT output parameters were derived for a total of 1589 MATLAS dwarf galaxies, yielding a morphological type mix of 1022 dE, 415 dE,N, 142 dI, and 10 dI,N (Poulain et al. 2021a). GALFIT modeling of 292 nuclei were also obtained.

3. MATLAS ultra diffuse galaxy sample

3.1. UDG Selection

Using the structural properties discussed in the previous section, the UDGs were selected using a cutout in effective radius of $R_e \geq 1.5$ kpc and surface brightness of $\mu_{0,g} \geq 24.0 \text{ mag arcsec}^{-2}$. This definition is adopted with no prejudice on whether they are a real class of objects or not, in order to allow comparison to the other similarly selected UDG samples. However, as can be seen already in Fig. 1, these selection criteria are somewhat arbitrary: the UDGs (green symbols) do not appear to represent a distinct

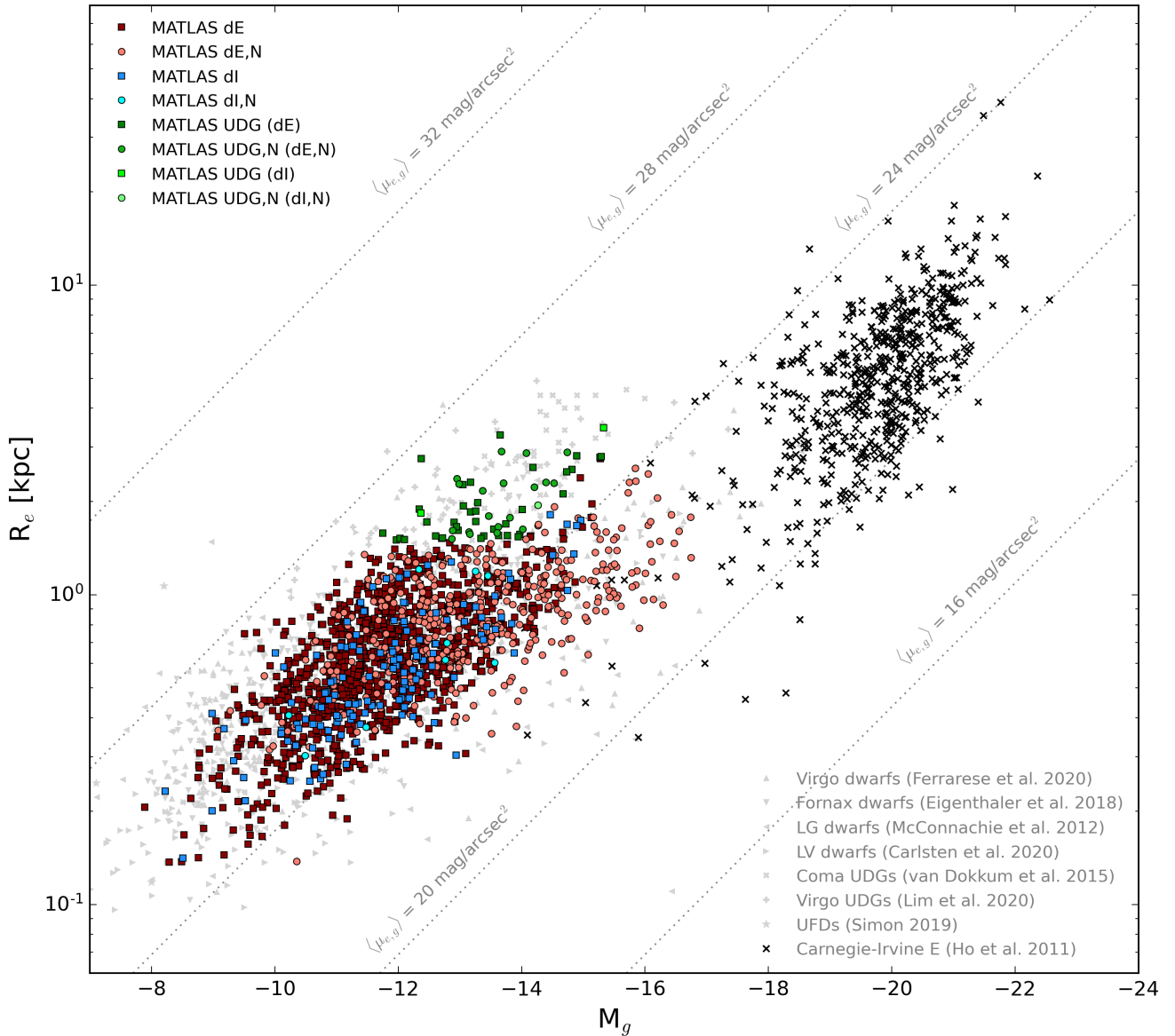


Fig. 1. Scaling relation M_g versus R_e for the MATLAS dwarfs and UDGs: The plotted quantities are based on parameters returned by the GALFIT modeling, and we have used the estimated distance to the dwarf when available and otherwise assumed that the dwarfs are at the same distance as the central ETG in the field. The nuclei of the dE,N have been fitted with a two-component (diffuse component and nucleus) model, and only the properties of the diffuse component of the galaxy are used here. The MATLAS dwarfs occupy the same parameter space as dwarfs identified in the NGVS (gray triangles; Ferrarese et al. 2020) and NGFS (inverted gray triangles; Eigenthaler et al. 2018) images, as well as Local Group dwarfs (rotated left gray triangles; McConnachie 2012) and Local Volume (rotated right gray triangles; Carlsten et al. 2020). The MATLAS UDGs occupy the same parameter space as the UDGs found in the Coma (gray cross symbols; van Dokkum et al. 2015) and Virgo cluster (gray plus symbols; Lim et al. 2020). The population of UDGs appear to simply be an extension in parameter space to the traditional dwarf population.

sequence of galaxies but rather an extension of the dwarf population in terms of effective radius and surface brightness.

Using this definition, we identify a total of 59 UDG candidates: 37 dE, 19 dE,N, 2 dI and 1 dI,N. Averaging over the surveyed area, we estimate that there are ~ 0.4 UDG per square degree. We note that this selection depends on the dwarf galaxy having a successful and reliable GALFIT result. Hence, it is possible that there are some UDGs amongst the MATLAS dwarfs that were not successfully modeled using GALFIT, in particular those (1) with an extremely low surface brightness (e.g., MATLAS-1830, Duc et al. 2014; see Sect. 7) and (2) classified as dIs since only 27% of the complete sample of MATLAS dIs were success-

fully modeled with GALFIT (compared to 87% of dEs) due to the presence of irregular features (Poulain et al. 2021a).

3.2. UDG distances

The identification of a UDG sample strongly depends on the accuracy of the distances to the candidates. Four UDGs in the sample defined above have available distance estimates: three have velocity measurements from HI data (one from the ATLAS^{3D} HI data cubes and two from the ALFALFA catalog) and one, MATLAS-2019, has a distance estimate based on the GCLF (Müller et al. 2021).

It is worth noting, given the general uncertainties in the distances to the remaining UDGs, that three of these four UDGs would still be classified as such if we adopted the distance to the assumed host, as defined in Sect. 2.2. For the other UDG, the assumed host had a distance of 19.1 Mpc, but the UDG actually lies at a distance of 35.9 Mpc according to the velocity extracted from the ALFALFA HI catalog. Conversely, we also have exactly one dwarf galaxy that would be classified as a UDG given the assumed distance of the host (37.1 Mpc), but had its physical size revised downward due to the distance estimate in the NEARGALCAT (10 Mpc).

Thus, in total, 4/59 of our UDG candidates have a distance estimate confirming their effective radii $R_e \geq 1.5$ kpc. Color (g, r, i) images of the 59 MATLAS UDGs in our final sample, ordered by increasing distance (19.1–46.3 Mpc), are shown in Fig. 2. The effective radius of the MATLAS UDGs ranges from 1.5 (our cut) to 3.5 kpc (see Fig. 1). As the distances of the UDGs are critical, we further explore the potential for misidentified host galaxies for the full UDG sample in Appendix A.

4. UDG environments

MATLAS specifically targeted the ATLAS^{3D} sample outside the Virgo cluster, which includes ETGs in groups, pairs, and isolated galaxies. A detailed study of the galaxy associations in the MATLAS fields is currently in progress (Smith et al., in prep.). For now, we calculate the local volume density ($\rho_N = 3N/4\pi r_{3D}^3$) and the surface density ($\Sigma_N = N/\pi r_{2D}^2$) using the $N = 10$ th nearest neighbor – in 3-dimensional and projected on-sky space, respectively – of each dwarf as a proxy for the local environment. We note that we considered only the massive galaxies from the ATLAS^{3D} parent catalog (ETGs and LTGs) when determining N ; to avoid large uncertainties for the 14 dwarfs known to lie at distances >50 Mpc, well beyond the ATLAS^{3D} sample, we have removed these few galaxies from the plot. The distribution is shown in Fig. 3.

In this plot, we have assumed that the dwarfs are at the same distance as the host galaxy, when no independent distance measurement is available. To estimate the error this introduces into $\log_{10}\rho_{10}$, we incorporated an offset of ± 500 km/s in velocity space, following the cut we used to define likely satellite/non-satellite dwarfs in Sect. 2.2, and propagated this through the calculations. We concatenated the \pm error estimates, and binned the data into four bins containing nearly equal number of datapoints in $\log_{10}\rho_{10}$ space: $\log_{10}\rho_{10} \leq -2.0$, $-2.0 < \log_{10}\rho_{10} \leq -1.58$, $-1.58 < \log_{10}\rho_{10} \leq -1.0$, and $\log_{10}\rho_{10} > -1.0$. In these four bins, the median errors are 0.01, 0.18, 0.28, and 0.4, respectively.

The UDGs can be found throughout the densities probed by the MATLAS sample, except for the lowest density regions, and follow a similar distribution as the dwarfs. Applying a two-sample Kolmogorov-Smirnov (KS) test, we find no statistically significant deviation in ρ_{10} between the sample of UDGs and the remainder of the MATLAS dwarfs sample, with a returned p -value of $p = 0.21$.

A number of groups with previously detected X-ray emission fall within the MATLAS fields and are also marked in the figure, to help gauge the local densities at various points in the plot. We note that while these open ovals enclose the dwarfs and UDGs associated with each group, the ovals themselves are illustrative and may enclose points that are not associated with the labeled group. The groups span a range of values in both ρ_{10} and Σ_{10} , depending in part on the relative position of the dwarf to the group center and the presence of substructures or nearby systems. For example, contamination from foreground galaxies in

the Virgo cluster increases Σ_{10} for NGC 4261 ($d \sim 31$ Mpc), while the proximity of NGC 4636 ($d \sim 16$ Mpc) to the Virgo cluster has increased ρ_{10} to cluster-like values for this group. In total, 19 UDGs (32.2%) lie within the virial radii of the groups with X-ray emission, while 484 dwarfs (22.5%; UDGs removed) lie within the same region.

4.1. Groups

Here we comment on the properties of those individual, and presumably massive, groups detected in X-rays. The group properties are summarized in Table 1. Spatial maps of all fields containing at least one MATLAS UDG are presented in Appendix B.

The NGC 3665 group. The NGC 3665 group is a loose association of approximately 10 galaxies, mainly late-type, with an anomalously low velocity dispersion (Helsdon et al. 2005). Approximately 40 new, potential dwarf group members have been identified in the MATLAS images, and we find one UDG located near the virial radius R_{vir} .

The NGC 4636 group. Located just south of the Virgo cluster at a distance of $d \sim 16$ Mpc (Kourkchi & Tully 2017), the NGC 4636 group is difficult to separate from the massive cluster. However, extended X-ray emission indicates that this group is a distinct structure. An analysis of the velocity dispersion of estimated members, and the position of the ETG NGC 4636 near the centroid of the group, suggest that it is a dynamically mature system (Brough et al. 2006). We identified 60 dwarfs within R_{vir} of the group, but none meet the selection criteria to be classified as a UDG. Nor are any UDGs found just outside R_{vir} .

The NGC 3607 group. Also known as the Leo II group or the Leo Cloud, this group is centered around two ETGs, NGC 3607 and NGC 3608. The group contains ~ 16 massive group members with total blue magnitudes brighter than $B \approx 16$, most of which are LTGs (Afanasiev & Silchenko 2007; Giuricin et al. 2000). The morphologies of the group members, the observation of hot X-ray gas maxima around both NGC 3607 and NGC 3608 within the common gaseous envelope (Mulchaey et al. 2003), and the presence of optical low-surface brightness features indicative of recent mergers within the group (Bílek et al. 2020) all suggest that this group is relatively young (Afanasiev & Silchenko 2007). We identify one UDG among the 37 dwarfs within the MATLAS footprint, but it should be noted that we do not have full coverage of the group within R_{vir} . The UDG is in close projection to the group center.

The NGC 0524 Group. The NGC 0524 galaxy group is a relatively isolated, low-richness group (O’Sullivan et al. 2017) with a higher-than-average fraction of early-type galaxies. The group appears to be dynamically mature (Brough et al. 2006) and a detailed study of the low surface brightness outskirts of the group members indicates that most are relaxed. Only NGC 0502 and NGC 0518 show evidence of past mergers (Bílek et al. 2020). We identified 62 dwarfs within the projected virial radius, but no UDGs. However, two UDGs can be found just outside the R_{vir} boundary and are likely associated with the group. Interestingly, both UDGs lie to the southeast of the group, in the direction of NGC 0502 – one of the two galaxies to have undergone a recent merger, although this may be a coincidence.

The NGC 5322 group. Optically, the NGC 5322 group is similar to NGC 4261, with similar B magnitudes, R_e



Fig. 2. Color (g, r, i) images of the 59 MATLAS UDGs in our final sample sorted by distance (from *top left* to *bottom right*, 19.1–46.3 Mpc). Each image is ~ 1 sq.arcmin. in size. North is up and east is left.

estimates, colors, color gradients, and the brightest group galaxy in each is classified as a Low-Ionization Nuclear Emission-line Region (LINER) galaxy. However, the NGC 5322 group exhibits a much fainter X-ray component, which has been interpreted

as disruption of the X-ray halo of a single galaxy due to a recent galaxy interaction or merger. The ETG NGC 5322 contains a counter-rotating core, further support of a recent merger (Finoguenov et al. 2006) and suggesting a younger group. We

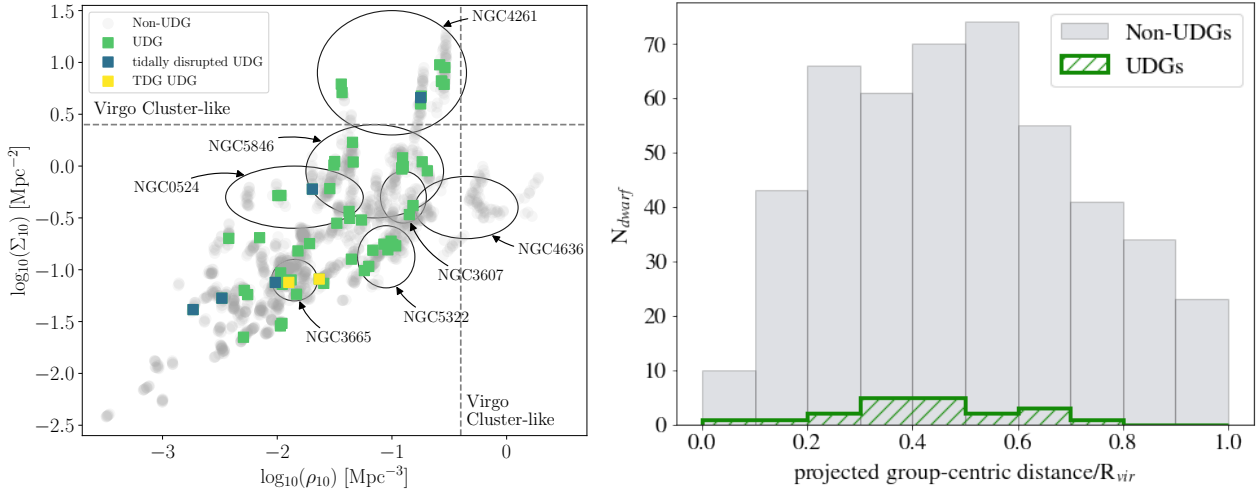


Fig. 3. *Left:* estimates of the local volume density (ρ_{10}) versus the local surface density (Σ_{10}) for the MATLAS traditional dwarf (non-UDG) galaxies (gray circles) and UDGs (green squares). The tidally disrupted UDGs and TDG UDGs discussed in Sect. 7 are marked in turquoise and yellow, respectively. The density estimates were calculated based on the tenth-nearest neighbor, using only the massive galaxies from the ATLAS^{3D} parent sample. Cappellari et al. (2011b) noted that nearly all galaxies in the Virgo cluster have $\log_{10}\rho_{10} > -0.4$ and $\log_{10}\Sigma_{10} > 0.4$; these boundaries are marked with dashed lines. The open ovals indicate where the dwarfs in select groups fall in the plot. *Right:* radial distribution of traditional dwarf (non-UDG) galaxies (filled gray) and UDGs (hashed green) in the group environments defined in Table 1. The projected group-centric distances have been normalized such that $R_{\text{vir}} = 1$. A KS test returns a p -value of 0.35, thus we cannot reject the null-hypothesis that the two samples originate from the same parent sample.

Table 1. Summary of known groups with X-ray detections that fall within the MATLAS images.

| Group | T | R | dist [Mpc] | R_{vir} [Mpc] | $\log(M_{\text{dyn}}/M_{\odot})$ | f_{cover} | N_{UDG} | $N_{\text{UDG,pred}}$ | N_{dwarfs} | f_{ETG} |
|----------|-----|-----|---------------|---------------------------|----------------------------------|--------------------|------------------|-------------------------|---------------------|------------------|
| NGC 3665 | G | L | 23.99 | 0.288 | 12.45 | 1.00 | 1 | $0.36^{+0.15}_{-0.29}$ | 44 | 0.28 |
| NGC 4636 | G | – | 16.20 | 0.472 | 12.93 | 0.41 | 0 | $1.23^{+0.39}_{-0.29}$ | 60 | 0.51 |
| NGC 3607 | G | – | 22.14 | 0.367 | 13.31 | 0.81 | 1 | $3.23^{+0.76}_{-0.29}$ | 37 | 0.41 |
| NGC 0524 | H | L | 31.19 | 0.388 | 13.13 | 0.98 | 0[+2] | $2.06^{+0.56}_{-0.29}$ | 62[+12] | 0.33 |
| NGC 5322 | H | L | 23.28 | 0.386 | 13.34 | 0.72 | 3[+2] | $3.5^{+0.8}_{-0.29}$ | 49[+19] | 0.38 |
| NGC 5846 | G | H | 26.74 | 0.596 | 13.75 | 0.64 | 7 | $9.95^{+1.51}_{-0.29}$ | 143 | 0.77 |
| NGC 4261 | G | H | 31.39 | 0.649 | 13.94 | 0.35 | 7 | $16.22^{+1.89}_{-0.29}$ | 89 | 0.54 |

Notes. The columns are: (1) the group name; (2) whether the X-ray emission is on group scales (G) or galaxy halo scales (H), taken from Osmond & Ponman (2004); (3) the richness of the sample: L=low richness, H=high richness, from O’Sullivan et al. (2017); (4) the distance to the group in Mpc, (5) projected virial radius in Mpc and (6) dynamical mass from Kourkchi & Tully (2017); (7) the fraction of the area within R covered by the MATLAS footprint; (8) the number of UDGs identified within R_{vir} – for two groups, we increased the search radius by 0.15 Mpc in order to catch the UDGs just outside the cluster bounds, which are included in brackets; (9) the number of predicted UDGs using the dynamical mass in Col. 6 and the relation described in van der Burg et al. (2017) – we note that this $N_{\text{UDG,pred}}$ value is nearly identical to the value returned by the relation in Janssens et al. (2019); (10) the number of MATLAS dwarfs (including UDGs) within R_{vir} – the numbers in brackets include the additional dwarfs found in a search radius increased by 0.15 Mpc; (11) the fraction of early-type galaxies in the group. For consistency, this fraction was calculated using the group membership and morphologies from Kourkchi & Tully (2017). The groups are ordered by increasing mass.

identified 49 dwarfs and three UDGs in this group. Like NGC 0524, however, there are an additional two UDGs a little beyond the virial radius, which we have noted in Table 1.

The NGC 5846 group. The NGC 5846 group is a massive and relatively isolated group at $d \sim 26$ Mpc. Mahdavi et al. (2005) note that the group has the third largest over-density of ETGs in the local Universe, after the Virgo and Fornax clusters. The group appears to have significant substructure, with two distinct subgroups centered on the ETGs NGC 5846 and NGC 5831. Nevertheless, the mass, high fraction of ETGs, and velocity dispersion of the group members suggest that this is a dynamically evolved group. It should be noted that low

luminosity members of the group have been studied previously (Mahdavi et al. 2005; Eigenthaler & Zeilinger 2010), and Mahdavi et al. noted that a few of the dwarfs in their sample are very low surface brightness objects, five of which are part of our UDG sample. In total, we have identified seven UDGs from the 143 dwarfs in the MATLAS footprint. One UDG candidate, MATLAS-2019, has been confirmed as a group member, and hence is a robust UDG, in individual case studies (Müller et al. 2020, 2021; Forbes et al. 2019, 2021).

The NGC 4261 Group. Also known as the W Cloud, NGC 4261 appears close in projection to the Virgo cluster, although it is more distant at $d \sim 31$ Mpc. It is thought that the

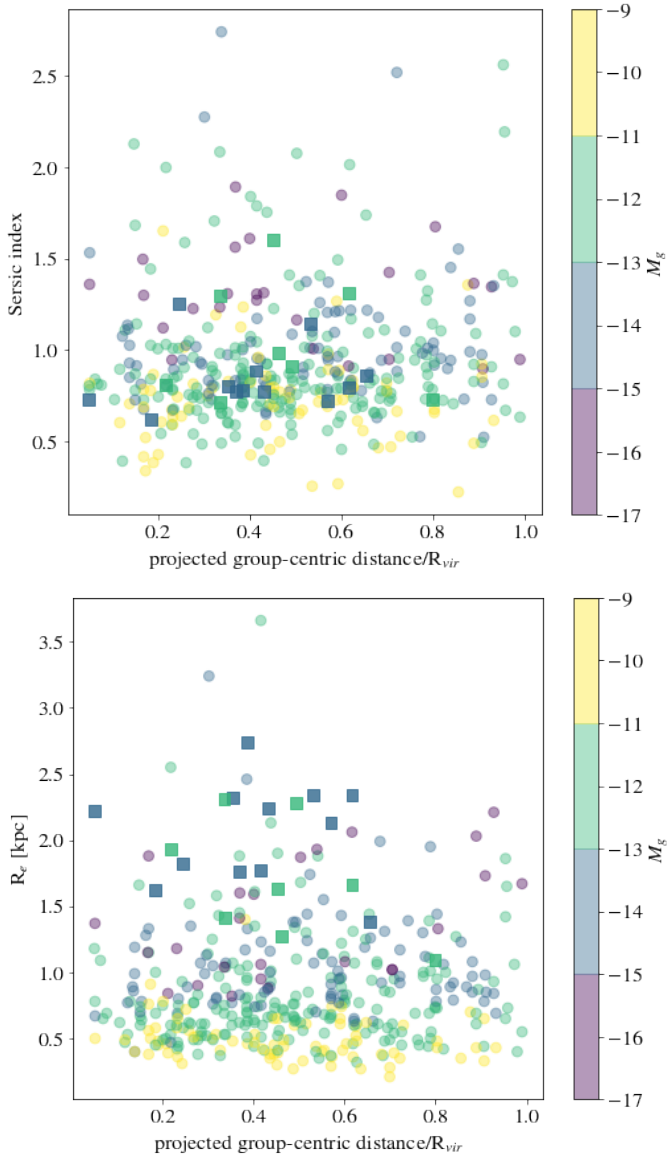


Fig. 4. Sérsic index (*top*) and physical size in kpc (*bottom*) as a function of group-centric distance for the traditional dwarf (non-UDG) galaxies (circles) and UDGs (squares). The colorbar represents the absolute g -band magnitude of the galaxies.

group may be part of a filament more or less along the line of sight, which is feeding into the cluster (Kourkchi & Tully 2017). The light profile of the group is unusual, with approximately half of the light found at radii $>0.75R_{\text{vir}}$; Helsdon & Ponman (2003) have interpreted this as evidence that galaxies are currently falling into the group. The central ETG, NGC 4261, also has signs of a minor merger in the past 1–2 Gyr (Bílek et al. 2020; O’Sullivan et al. 2011). Taken together, these suggest that the group is fairly young.

The proximity of the Virgo cluster makes it difficult to determine group membership, and the association of the 82 traditional dwarf (non-UDG) galaxies and 7 UDGs may also be suspect. We can estimate the contamination from the LSB Virgo cluster members in this region of the sky statistically, however. Figure 4 from Roberts et al. (2007) shows the number density of dwarfs as a function of cluster-centric distance, measured in two directions that avoid the various substructures in the cluster. Taking the larger of the two estimates gives a number density of roughly

10 LSB dwarfs per square degree at the distance of NGC 4261. Thus, we would expect approximately 15 of our dwarfs (18%) to be members of the foreground Virgo cluster rather than the NGC 4261 group. We note that if any of our UDG candidates are at the distance of the Virgo cluster, they would be classified as normal dwarf galaxies. The largest of the UDG candidates would have a recalculated $R_e = 1.16$ kpc. Without further confirmation, however, we retain the current distance estimate for these dwarfs, that is, $d \sim 31$ Mpc.

The traditional dwarfs and UDGs within the projected virial radii of the known X-ray groups can be stacked to better understand trends of these systems within groups. In Fig. 3, (right), we plot the distribution of projected group-centric distance for both the traditional dwarf (non-UDGs) galaxies and the UDGs, where the virial radius of each group has been scaled such that $R_{\text{vir}} = 1$. The traditional dwarf (non-UDG) galaxies are spread fairly uniformly throughout the groups. The distribution of UDGs is similar, and we cannot reject the null hypothesis that the two distributions arise from the same parent distribution via a two sample KS test with a p -value $p = 0.35$.

The distribution of UDGs in individual groups varies greatly. For example, in NGC 5846, many of the UDGs appear close in projection to the center of the group, while the two UDGs associated with NGC 0524 are found just outside the virial radius. The expected distribution of UDGs is not clear. van der Burg et al. (2016) found that the projected radial distribution of UDGs in clusters is well fit by an Einasto profile, with a steep profile in the cluster outskirts that flattens toward the cluster center. It should be noted that the regular dwarfs in that study do not follow the same distribution, at least in the central regions. However, Lim et al. (2020) found that UDGs in the Virgo cluster are more centrally concentrated than other galaxies with similar magnitudes. In a study of UDGs in the Frontier Fields (Janssens et al. 2019), the authors note that the UDGs in individual clusters often show lopsided distributions, with the exception of the most relaxed cluster in the sample, where the distribution is roughly uniform. Given the uncertainties in the expected UDG distribution, and whether that distribution would apply equally to groups as clusters, we have made no attempt to correct the number of UDGs in the X-ray groups for incomplete MATLAS coverage. However, this fraction is noted in Table 1.

In Figs. 4 and 5, we plot the Sérsic index, R_e , and colors of the dwarfs and UDGs as a function of the group-centric distance and absolute magnitude. The effective radius and absolute magnitudes were recalculated assuming the group distance given in Table 1; this was applied to the dwarfs/UDGs with independent distance estimates as well, to avoid uncertainties in the distance due to relative motions of the satellites. It should be noted that this results in minor changes to the sample; the recalculated effective radii of four UDGs (Fig. 4 bottom, squares) is lower than $R_e = 1.5$, while 16 traditional dwarf (non-UDGs) galaxies (Fig. 4 bottom, circles) with $\mu_{0,g} \geq 24.0$ mag arcsec $^{-2}$ now have $R_e \geq 1.5$ kpc; we note, however, that these 16 galaxies are not distinguished from the other traditional dwarfs with brighter μ_0 in the plot. None of the 20 galaxies which would be reclassified as a UDG or non-UDG have robust distance measurements available. As the association of the galaxies with the groups has not been proved, the group distance estimate is no more certain than the central ETG in the field distance estimate previously assumed, and we will not update our sample of 59 UDGs until more accurate distances are obtained.

The distribution of the UDGs and traditional dwarfs is similar in both Figs. 4 and 5. We do not see a systematic offset

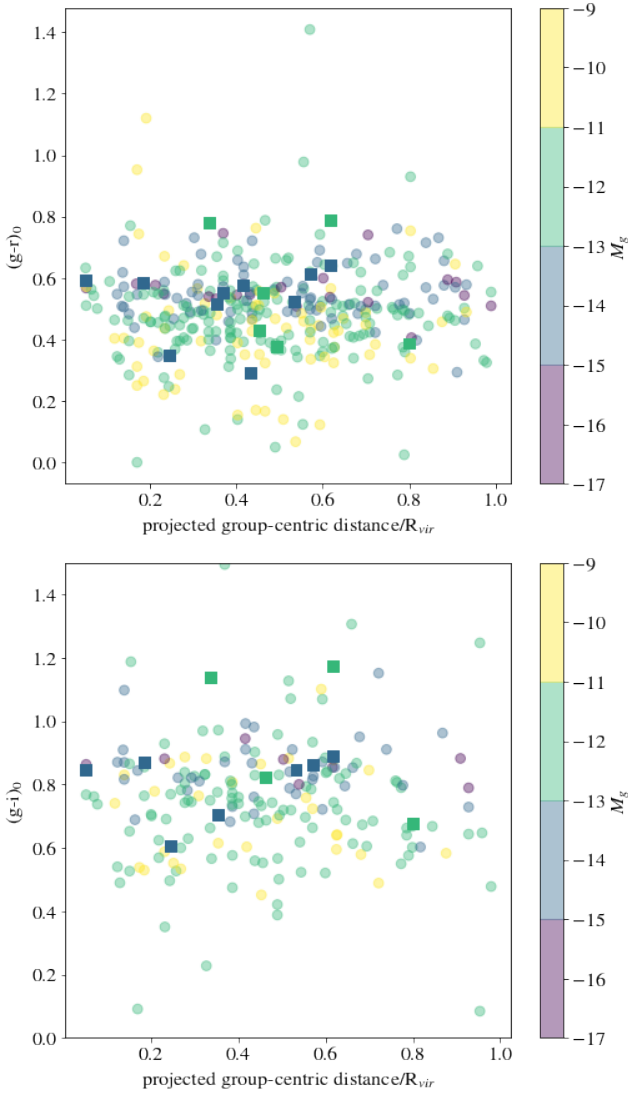


Fig. 5. $(g-r)_0$ color (*top*), and $(g-i)_0$ color (*bottom*) as a function of group-centric distance for the traditional dwarf (non-UDG) galaxies (circles) and UDGs (squares). The colorbar represents the absolute g -band magnitude of the galaxies.

between the UDGs and the traditional dwarfs, aside from a separation in R_e between the UDGs and the bulk of the group dwarfs (Fig. 4, bottom), which is simply by the construction of the UDG definition; even here, however, there are a number of traditional dwarfs with UDG-like sizes, but which have central surface brightness $\mu_{0,g} < 24.0$ mag arcsec $^{-2}$. We also do not observe any trends with group-centric distance among the four parameters, except for a possible color shift toward the blue with increasing distance from the group center. It should be noted, however, that using the projected distances may erase the signature of any radial trends. A more rigorous analysis must wait until distances estimates for a large number of the traditional dwarfs and UDGs are obtained.

4.2. Other galaxy associations

In addition to the groups with observed X-ray emission discussed above, the MATLAS images contain a number of groups and galaxy associations that have been identified in other wave-

lengths. To identify other associations, we searched for groups in the Kourkchi & Tully (2017) groups catalog. This catalog is based on an all-sky sample of $\sim 15\,000$ galaxies with $V_{LS} < 3500$ km s $^{-1}$, where V_{LS} is the radial velocity relative to the Local Sheet. The groups were identified through a galaxy linkage program using known scaling relations. These authors placed a particular emphasis on small groups, and the catalog contains a number of groups with fewer than three members. The X-ray groups discussed above are all contained within the catalog, and when we expand the search to include all groups with $R_{vir} < 1.5$ deg, to focus on the local environment, we find that 61% of the UDGs fall within the virial radii of one of the Kourkchi & Tully (2017) groups, and 81% are enclosed within $1.5R_{vir}$. In comparison, 58% of the non-UDG dwarfs lie within $1R_{vir}$ and 70% lie within $1.5R_{vir}$.

These additional optical groups each have between 0–3 UDGs. As with the X-ray groups, we find that the more massive groups are more likely to host a UDG, in agreement with previous work by Janssens et al. (2019) and van der Burg et al. (2017). In particular, we note a rough break at $\log(M_{dyn}/M_{\odot}) \sim 12.5$; below this value, only 4/43 groups contain at least one UDG, while above this cut 16/35 groups have 1+ UDGs within R_{vir} . At the high mass end, however, we are likely underestimating the fraction of groups with associated UDGs; the more massive groups typically also have larger R_{vir} , and the MATLAS footprint may not be large enough to observe UDGs on the outskirts or a lopsided distribution. The least massive system with at least one UDG within the estimated virial radius, the NGC 772/NGC 770 pair, has $\log(M_{dyn}/M_{\odot}) = 11.88$ and has two UDGs.

The MATLAS images also include the Hickson 44 group, which is dominated by three LTGs and one ETG, although there is some debate if the ETG is part of the group or an isolated background galaxy. The morphologies of the group members, along with a lack of X-ray emission or intra-galactic light, suggests that this is a dynamically young system (Aguerri et al. 2006). Smith Castelli et al. (2016) identified two UDG candidates in this field, although neither is included in our sample; one is in the halo of the ETG, while the other is near a bright star. Neither UDG could be deblended from the surrounding emission on the MATLAS images, either by eye or with SEXTRACTOR. This group is mentioned here for completeness, and to highlight another dynamically young group with UDGs.

4.3. Isolated hosts

Defining a galaxy as isolated without a full kinematic analysis of its nearest neighbors is somewhat subjective, and a number of UDGs are located near likely galaxy pairs and triplets that are not part of the Kourkchi & Tully catalog. Nevertheless, a small number of UDGs appear to be associated with relatively isolated ETGs – ETGs that are not associated with a Kourkchi & Tully group and have no massive galaxies (ETGs or LTGs from the ATLAS 3D parent sample) in their vicinity. Examples include: IC 0560, NGC 1248, NGC 5493, and UGC 4551. Each of these galaxies has at most one associated UDG in our sample. Two of the four UDGs show evidence for tidal interactions (see Sect. 7), while only one of the hosts (NGC 5493) shows clear evidence that it has undergone an old major merger; the other hosts are relaxed, although IC 0560 is surrounded by bright stellar halos that may have masked such faint features (Bilek et al. 2020). These ETGs have stellar masses, estimated from the K -band luminosity, that span the range $10.15 < \log(M_*/M_{\odot}) < 11.25$.

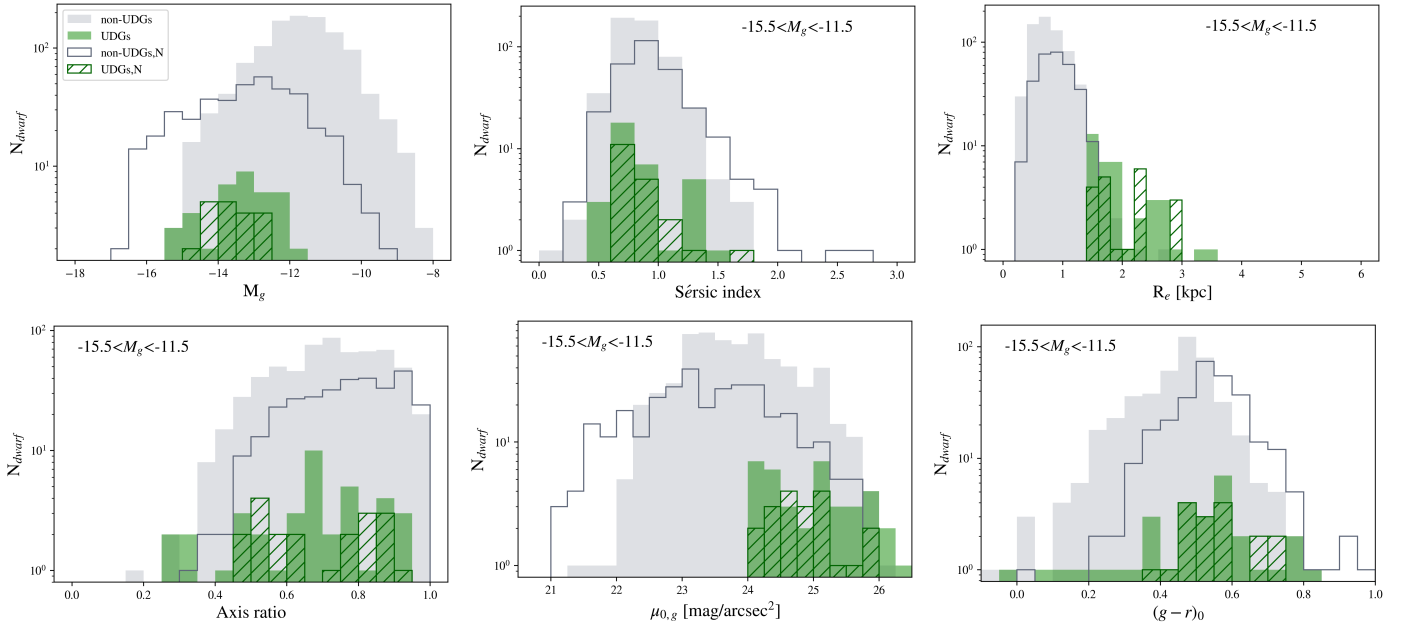


Fig. 6. Comparison of distribution of photometric and structural properties – absolute magnitude M_g , Sérsic index n , effective radius R_e , axis ratio, central surface brightness $\mu_{0,g}$, and $(g-i)_0$ color – between the UDGs (green) and the non-UDGs (gray) in the MATLAS dwarfs sample. The samples are divided by nucleation status: nucleated (empty gray/hashed green) and nonnucleated (filled gray/green). All dwarfs are shown for M_g while only galaxies in the range of the UDGs luminosity, $-15.5 < M_g < -11.5$, are considered for the other parameters.

There is one potentially isolated ETG, NGC 4690, which has two UDGs in close projection. However, all three galaxies are near the R_{vir} boundary of two other groups, thus the ‘isolated’ classification of these galaxies is suspect. NGC 4690 shows evidence for a recent minor merger; neither of the UDGs display any tidal features.

5. UDG photometric properties

5.1. Photometry and structural parameters

In Fig. 6 we display the Sérsic index, effective radius, absolute magnitude, axis ratio and $(g-i)_0$ color distribution of the UDGs, as compared to the traditional dwarf (non-UDGs) galaxy sample. We note that when we compare the photometric and structural properties of these two samples, we compare galaxies of similar luminosity and therefore we only consider the range of luminosities where the two populations overlap, that is, $-15.5 < M_g < -11.5$. Other than the effective radius and the central surface brightness, which, by definition shows that the UDGs are selectively larger in size and fainter, the UDGs reach smaller values of Sérsic index but have similar range of axis ratios and colors than that of the traditional dwarf (non-UDGs) galaxy sample.

We compare in Fig. 7 the structural parameters of our UDGs with those located in the high density environments of clusters (Coma; Zaritsky et al. 2019, Virgo; Lim et al. 2020, Abell 168; Román & Trujillo 2017a and Hydra I; Iodice et al. 2020) and in moderate to low density environments (around NGC5485: Merritt et al. 2016, around IC 1459: Forbes et al. 2020, around HCG 07, HCG 25 and HCG 98: Román & Trujillo 2017b, and in the field: Greco et al. 2018; Leisman et al. 2017). For the comparison, we use the absolute magnitude range of $-15.1 < M_g < -13.0$ that is common to all clusters. We note that a different cut in size and surface brightness was applied to select the UDG samples in Greco et al. (2018), Lim et al. (2020),

Zaritsky et al. (2019), Román & Trujillo (2017b), Leisman et al. (2017). Focusing on the Sérsic index, the MATLAS UDGs have a larger minimum value than the Abell 168 cluster UDGs but similar to Hydra I cluster and the low density environment UDGs. This highlight a possible trend for the UDGs in low density environments to have a brighter center than the UDGs in the high density environments. Mancera Piña et al. (2019) studied a sample of 442 UDGs located in eight nearby clusters ($z < 0.035$). We compare the ranges of Sérsic index found for all eight clusters and find a similar tendency to the Abell 168 cluster, as the MATLAS UDGs minimum value is larger than the minimum indices of five clusters. And we also observe this trend by comparing our sample to the UDGs located in the Abell 370 cluster (Lee et al. 2020). However, we do not observe any relation between the Sérsic index and the local volume density ρ_{10} of the MATLAS UDG. Now, looking at the distributions for the axis ratio, we observe similar ranges for all the samples. Concerning the luminosity and the size of the UDGs, the MATLAS UDGs have R_e below 3.5 kpc. For a similar range of M_g (-15.5 to -11.5), the Coma cluster has a few larger UDGs, reaching 12.6 kpc, and two UDGs, one in the Virgo cluster and one around NGC 5485, have $R_e \sim 5$ kpc while the other samples show ranges in R_e similar to MATLAS.

The detection of the dwarfs was based solely on the g -band imaging, but magnitudes were obtained using GALFIT on the g -, r - and i -band images, allowing us to extract $g-r$ and $g-i$ colors for 1307 and 782 MATLAS dwarfs, including 49 UDGs, respectively. We extracted the magnitudes in the r - and i -bands of all the dwarfs having an available observation and a good model in the g -band with the use of GALFIT. We used the same model as in the g -band, leaving only the magnitude free to change for the initial input parameters of GALFIT. For the nucleated galaxies, the galaxy and nucleus was modeled and photometry was extracted separately (Poulain et al. 2021a).

The magnitudes were corrected for Galactic extinction that were obtained from the IRSA database at the coordinates of each

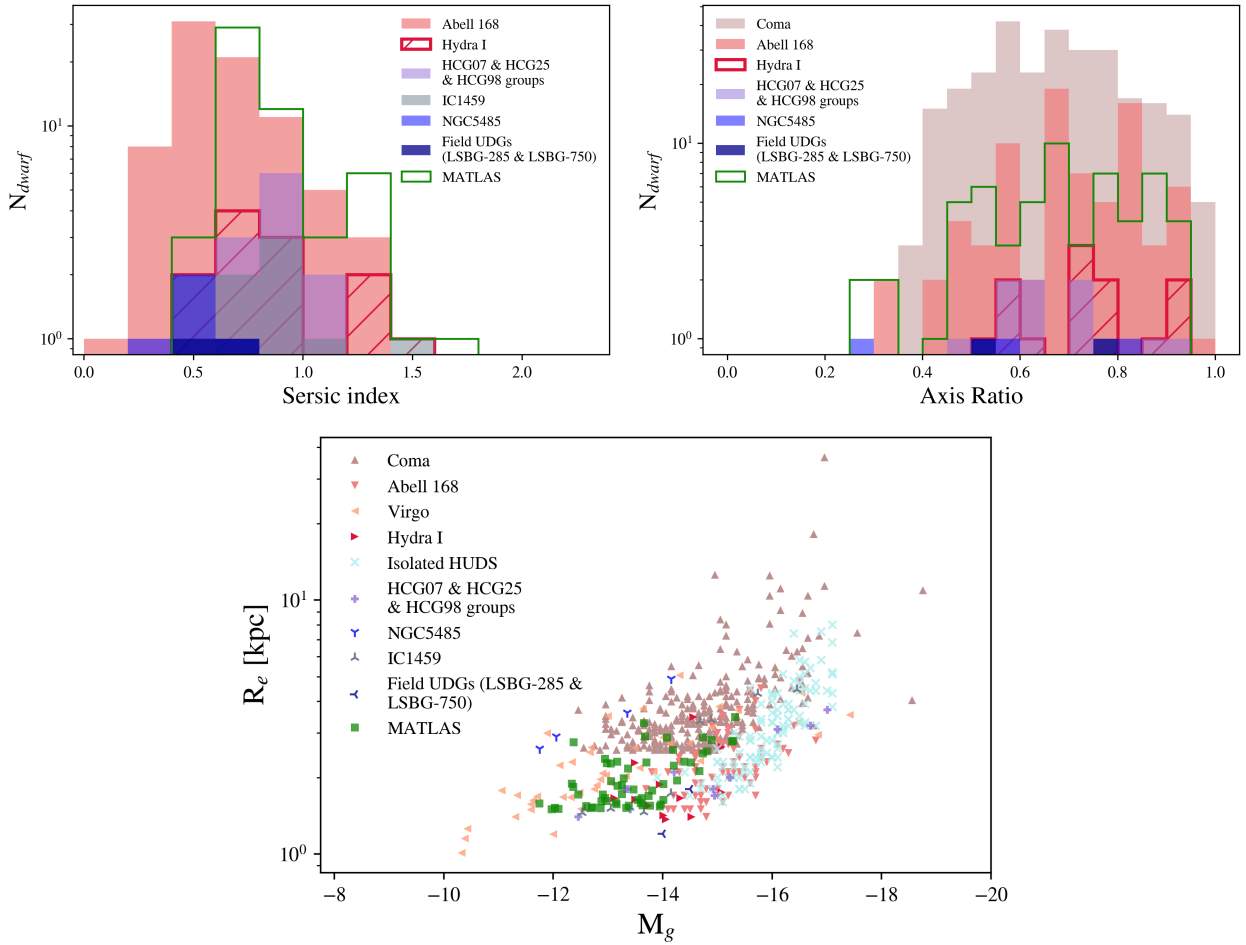


Fig. 7. Structural properties of the MATLAS UDGs as compared to the ones of UDGs from the Coma, Abell 168, Virgo and Hydra I clusters (Zaritsky et al. 2019; Román & Trujillo 2017a; Lim et al. 2020; Iodice et al. 2020), from the HCG 07, HCG 25, HCG 98, IC 1459 and NGC 5485 groups (Román & Trujillo 2017b; Forbes et al. 2020; Merritt et al. 2016) as well as of isolated UDGs (HI-bearing UDGs sample, LSBG-285 and LSBG-750, Leisman et al. 2017; Greco et al. 2018). We display the UDGs from high density (cluster) environments with shades of red and triangular markers, the UDGs from moderate (group) to low (field) density environments with shades of blue and cross-like markers and the MATLAS UDGs with a green cut in size and surface brightness was applied to select the UDG samples in Greco et al. (2018), Lim et al. (2020), Zaritsky et al. (2019), Román & Trujillo (2017b), Leisman et al. (2017).

dwarf, using the reddening values from Schlafly & Finkbeiner (2011) and assuming $R_V = 3.1$. The median g , r , and i -bands extinction corrections are 0.09, 0.06, and 0.04, respectively. Applying these corrections, we measure median colors $(g - r)_0 = 0.48$ and $(g - i)_0 = 0.73$ for the full dwarf sample and $(g - r)_0 = 0.49$ and $(g - i)_0 = 0.74$ for the traditional dwarf (non-UDG) galaxies.

The color of UDGs have been previously reported to depend on their environment. In the Coma cluster, they appear to follow the red sequence (Koda et al. 2015), while they show bluer colors in the outskirts of groups (Román & Trujillo 2017b) as well as blue colors and star forming activity in the field (Prole et al. 2019b). In Fig. 8 we compare the colors of our UDGs to the MATLAS traditional dwarf (non-UDGs) sample and to the samples of UDGs from Fig. 7 with available $g - r$ or $g - i$ color. Our UDGs have colors in the same range as the MATLAS traditional dwarf (non-UDGs) galaxies, which show red to blue colors, with $(g - r)_0 = -0.1$ to 0.8 and $(g - i)_0 = -0.2$ to 1.2. No UDG catalogs in the cluster environment had available $g - i$ color, allowing us to compare our UDG sample (Fig. 8, green squares) with low density environment UDGs only (Fig. 8, various blue markers).

We find that some MATLAS UDGs are as blue as the bluest UDGs (in IC1459) while other MATLAS UDGs are redder than the reddest UDG of the low density environment samples.

We can compare the MATLAS UDGs (Fig. 8, green squares) to the one in the Coma and Hydra I clusters (Fig. 8, various red markers) using $g - r$ color, in addition to samples of UDGs from low density environments (Fig. 8, various blue markers). In this color-magnitude diagram, the MATLAS UDGs show a similar range of color to the ones from other low density environments while we find some bluer and redder UDGs in the Coma cluster. The median color of UDGs in the MATLAS sample, $(g - r)_0 = 0.36$, is as red as the one measured in Coma, $(g - r)_0 = 0.40$, but the range of colors is narrower. The Hydra I cluster median color is redder, with $(g - r)_0 = 0.57$, and the UDGs are as red as the red UDGs from low density environments while they do not show as blue UDGs.

In summary, other than the predefined size and surface brightness cut, the MATLAS UDGs do not appear to have significantly different photometric and structural properties than the traditional dwarf (non-UDGs) galaxies. They also show similar colors than the MATLAS traditional dwarf (non-UDGs)

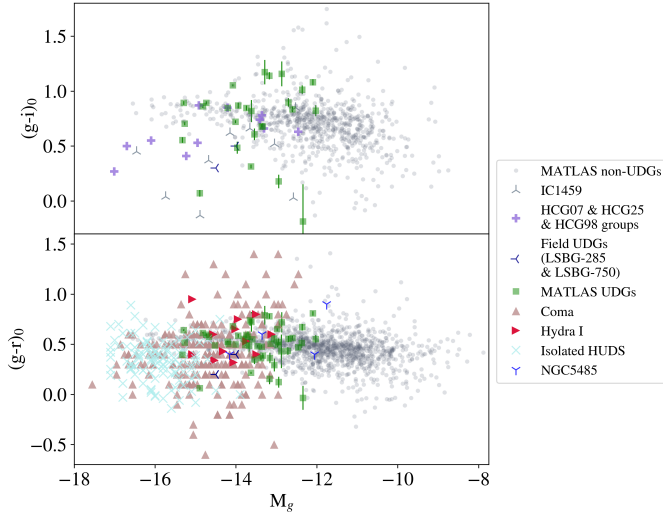


Fig. 8. *Top:* $(g-i)_0$ color as a function of the M_g for the MATLAS non-UDGs (gray dots) and UDGs (green squares) compared to UDGs located in groups and in the field (cross-like blue markers). *Bottom:* $(g-r)_0$ color as a function of M_g for the MATLAS non-UDGs (gray dots) and UDGs (green squares) as compared to UDGs located in the Coma and Hydra I clusters (red triangles), in groups and in the field (cross-like blue markers). The lines of markers visible for Coma’s $g-r$ color are due to the rounded absolute magnitudes used for the calculation.

galaxies in groups and in the field. Their median color is as red as the one measured in galaxy clusters such as Coma, but the range of colors is narrower. A table of the photometric properties of the MATLAS UDGs can be found in Appendix C.

5.2. Nucleated

During the visual classification of the 2210 MATLAS dwarf galaxies, 507 nucleated dwarfs (22.9%) were identified. Considering only those with GALFIT parameters, 425 (26.7%) are nucleated. We define a nucleus as a compact source within $\sim 0.5R_e$ of the dwarf photocenter, that appears to be the brightest compact source within the dwarf’s effective radius. In the UDG sample, we find 20 nucleated, leading to a nucleated fraction of 33.9%. One of these is irregular in morphology while the others are ellipticals. The nucleated fraction of the UDGs is similar to the one found in the Coma and Hydra I clusters (Lim et al. 2018; Iodice et al. 2020). Looking at the dwarfs with M_g in the range of the UDGs luminosity (-15.5 to -11.5), the nucleated fraction of non-UDGs is 33.8%, similar to the nucleated fraction of the UDGs. The nucleated fraction of dwarf galaxies depends on the galaxy mass and environment (Lim et al. 2018; Sánchez-Janssen et al. 2019). We know that the nucleated fraction of the MATLAS dwarfs is higher in more massive galaxies and that, for a similar stellar mass, the fraction is systematically lower than the nucleated fraction found in the Virgo cluster (Poulain et al. 2021a). We investigate the effect of the environment on the nucleated fraction of the MATLAS dwarfs non-UDGs and UDGs by using the local volume density ρ_{10} . We show the relation between the nucleated fraction and ρ_{10} in Fig. 9. We can see, as expected, an increase of the fraction toward higher local density environment for the non-UDGs. The same increase is seen only in the lowest two bins for the UDGs. Lim et al. (2018) found that the fraction of nucleated UDGs is lower than the one of the dwarfs at the center of the Coma cluster. We observe a tendency for the

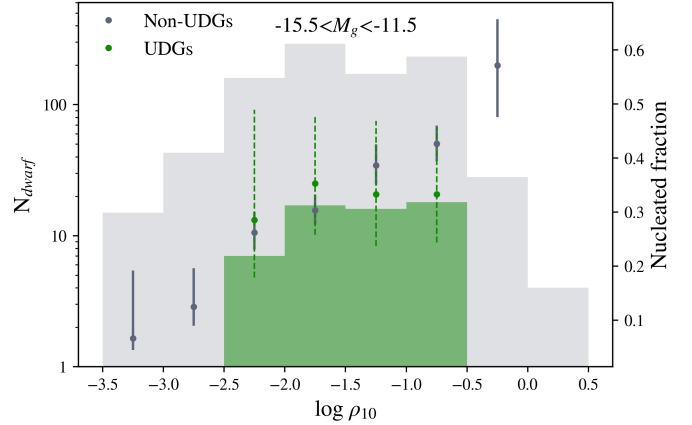


Fig. 9. Histograms: UDG (green) and non-UDGs (gray) counts in each ρ_{10} bin. We computed the fraction for bins of at least five galaxies. Points: nucleated fraction as a function of the local volume density ρ_{10} of the UDGs (green squares) and non-UDGs (gray dots). Error bars: 1σ binomial confidence intervals. Only galaxies in the range of the UDGs luminosity, $-15.5 < M_g < -11.5$, are considered in this analysis.

nucleated fraction of the UDGs to be larger than the one for the non-UDGs in the lowest density environments while it appears to be lower in the highest density environments. We note however that if we consider the error bars, the fractions of both samples are in agreement in most of the density bins.

We investigate the properties of the UDG nuclei, as compared to the nuclei in the traditional dwarf (non-UDGs) galaxies. We look at the UDG nuclei offset from the host galaxy photometric center. We show in Fig. 10 this separation both in units arcseconds and fraction of the galaxy R_e as a function of the galaxy M_g . All the UDG nuclei are located within $\sim 0.2R_e$ [$\sim 3''$] with a median separation of $0.06R_e$ [$1''$]. The median angular offset is larger than the angular offset of non-UDGs of similar luminosity ($0.36''$), but in units of R_e , both samples are similar ($0.06R_e$). We now focus on the nuclei luminosity by considering the contribution of the nucleus to the total luminosity of the galaxy and the nuclei M_g (Fig. 11). Considering galaxies of similar luminosity ($-15.5 < M_g < -11.5$), while we find a maximum contribution much larger for the traditional dwarf (non-UDGs) galaxies than for the UDGs (44.8% compared to 5.5%), the median contributions of the UDGs and non-UDGs nuclei are similar. Moreover, we observe on average brighter nuclei in the UDGs than in the non-UDGs. Forbes et al. (2020) report two single nucleated and one double nucleated UDGs in the IC1459 group which nuclei show redder colors than the galaxies. Figure 12 compares the $(g-i)_0$ and $(g-r)_0$ colors of the galaxy to the colors of the nuclei for the MATLAS non-UDGs and UDGs samples. While we find both bluer and redder nuclei in the traditional dwarf sample, we observe a tendency of the nuclei to be bluer than the galaxy in the case of the UDGs.

5.3. Stellar masses

Using the colors above and the distance – taken to be the dwarf distance when available, otherwise the ETG distance is assumed – it is possible to estimate their stellar masses. We computed the stellar masses M_* based on the stellar mass-to-light ratios from Bell et al. (2003) and the derived $(g-r)_0$ color¹. Stellar masses were measured for 1307 dwarfs, including 49 UDGs.

¹ Formula: $\log(M_*/M_\odot) = -0.306 + 1.097(g-r)_0 - 0.4(M_r - 4.77)$.

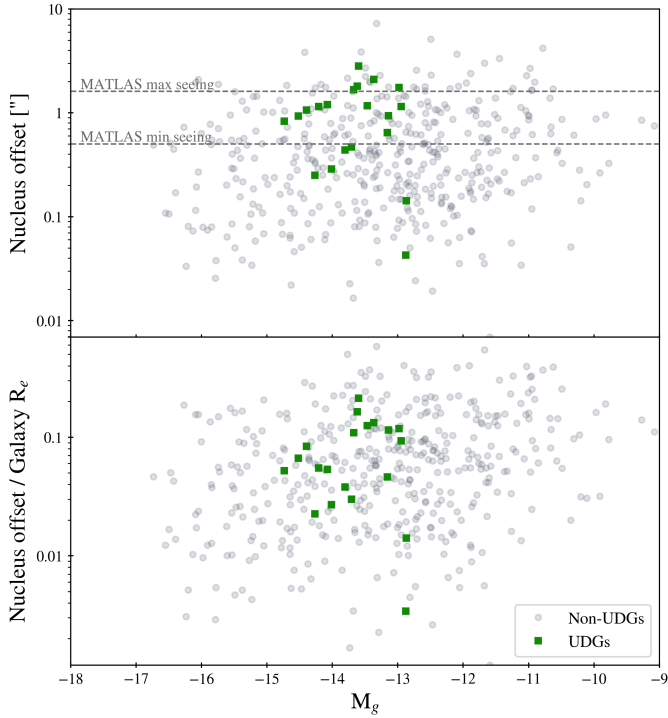


Fig. 10. Distribution of the estimate offset distance between the photometric center of the host galaxy and the nucleus as a function of the absolute magnitude M_g of the host. *Top*: offset in arcseconds. *Bottom*: offset in fraction of R_e of the host.

The distributions of stellar masses for the MATLAS traditional dwarf (non-UDGs) galaxies and UDGs with GALFIT parameters and $g - r$ colors are shown in Fig. 13. As expected, the MATLAS UDGs represent a subsample of the massive dwarfs, but not the most massive ones which are all nucleated non-UDGs. With stellar masses ranging from $\log(M_*) \sim 6.5$ to $\log(M_*) \sim 8.7$, the MATLAS UDGs have similar masses to UDGs observed in the field, groups and clusters ($\log(M_*) \sim 6.8$ – 8.6 , [Barbosa et al. 2020](#); [Greco et al. 2018](#); [Leisman et al. 2017](#); [Forbes et al. 2020](#); [Mancera Piña et al. 2019](#)).

6. UDG globular cluster populations

6.1. Catalog

The GC system of UDGs provides important clues on their stellar population and the nature of their dark matter halo. In particular, the stellar population of GCs provides information about the early epoch of galaxy formation when intense star formation occurred and massive star clusters were formed. They can be used as a means of estimating the total mass of a galaxy based solely on photometric measures since the number of GCs in a galaxy has been found to correlate linearly with the total host halo mass (e.g., [Blakeslee 1999](#); [Spitler & Forbes 2009](#); [Georgiev et al. 2010](#); [Hudson et al. 2014](#); [Harris et al. 2013, 2017](#); [Burkert & Forbes 2020](#)). Assuming that the GCs trace the underlying gravitational potential, are in dynamical equilibrium, and are pressure-support dominated, their velocity dispersion can also be used to estimate the total mass of the system ([Doppel et al. 2021](#); [Toloba et al. 2018](#); [Forbes et al. 2017](#); [Alabi et al. 2016](#); [Zhu et al. 2014](#); [Woodley et al. 2007](#)).

We studied the GC population of the MATLAS UDGs by selecting GC candidates on the basis of their colors and size

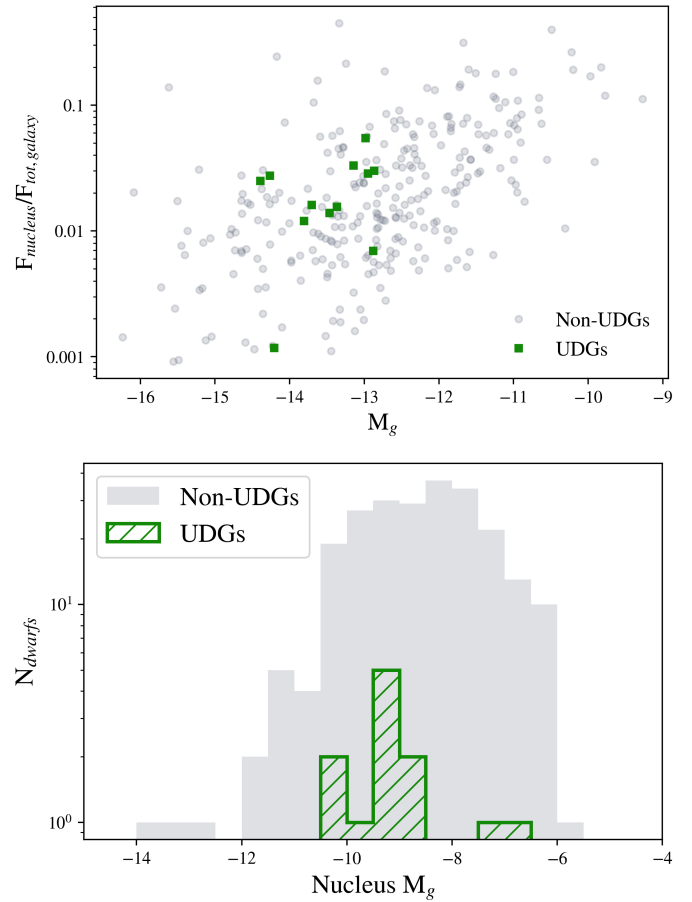


Fig. 11. Luminosity of MATLAS UDGs nuclei as compared with the ones of the MATLAS dwarfs. *Top*: contribution of the nucleus to the total luminosity of the galaxy as a function of the galaxy absolute magnitude. *Bottom*: distribution of absolute magnitude of the nuclei of the MATLAS dwarfs and UDGs. No difference in luminosity is visible between the UDGs and dwarfs nuclei.

information using the SExtractor package (see [Durrell et al. 2014](#); [Muñoz et al. 2014](#); [Lim et al. 2017](#)). The GCs at the distances of MATLAS UDGs appear as point-like sources, so we selected point-like sources based on concentration indices (Δ_{4-8}), that is, the difference between four- and eight-pixel diameter aperture-corrected magnitudes. We estimated Δ_{4-8} on the two best seeing filter images in each field and convolved the Δ_{4-8} values. If the seeing of the second best seeing image was greater than 1.3 times the one of the best seeing image, then we only used Δ_{4-8} from the best seeing image. We chose objects with $-0.08 < \Delta_{4-8} < 0.08$ range for most MATLAS dwarfs, but we used $-0.08 < \Delta_{4-8} < 0.16$ range for distances closer than 20 Mpc and seeing better than 1 arcsec. Among these point-like sources we chose GCs using their color information, (u, g, i) , (g, r, i) , or (g, r) , depending on the bands available (see Sect. 2.1). The colors of spectroscopically confirmed GCs in M87 were used as references of GC color regions (see [Muñoz et al. 2014](#); [Lim et al. 2017](#) for details). We limited our GC candidates to brighter than g -band magnitudes 24.5 in most fields, and we used $m_g \leq 24.0$ for GC candidates in fields which only have two-band data. For some low image-quality fields (seeing greater than 1.1 arcsec), we limited our GC candidates to those with $m_g \leq 23.5$.

In total, GCs were detected in 136 of the 150 fields, with only 14 fields missing due to problems in the images.

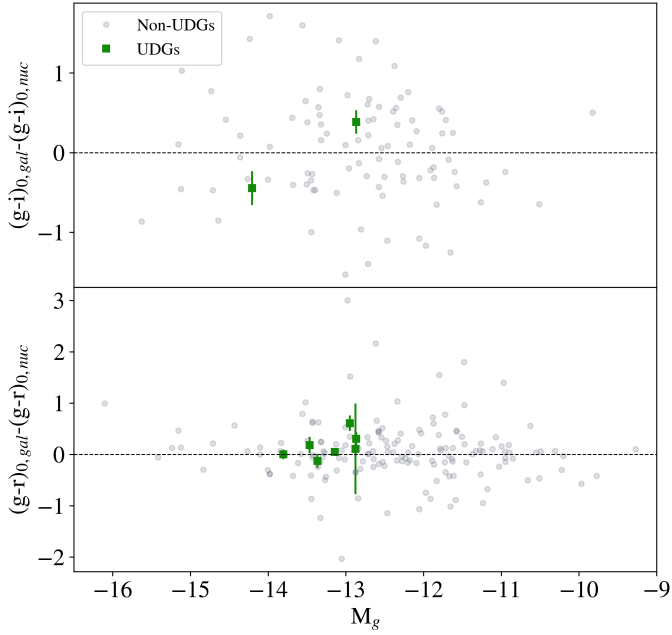


Fig. 12. Difference of color between the galaxy and the nucleus for the MATLAS non-UDGs (gray dots) and UDGs (green squares). *Top:* $(g-i)_0$ color. *Bottom:* $(g-r)_0$ color. The black dashed lines represent equal colors for the galaxy and nucleus. We see a tendency for the nucleus to be bluer than the galaxy in the case of the UDGs.

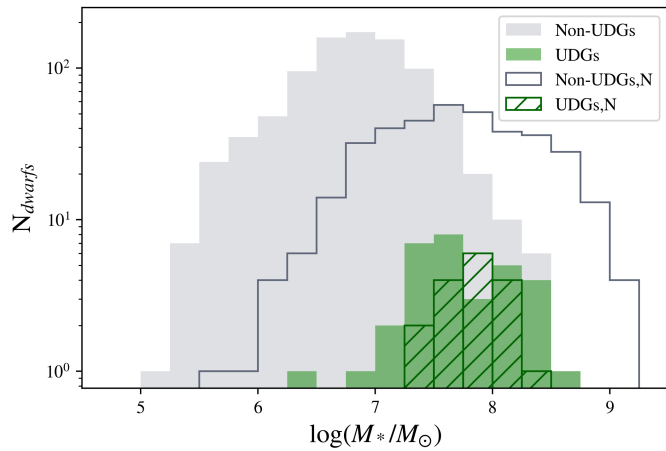


Fig. 13. Distribution of stellar masses for the 49 UDGs (green) and 1258 traditional dwarf (non-UDGs) galaxies (gray) with GALFIT parameters and $(g-r)$ colors, based on the Bell et al. (2003) color-mass relation. The samples are divided by nucleation status: nucleated (empty gray/hashed green) and nonnucleated (filled gray/green).

We cross-checked our final GC catalog with the *Gaia* DR2 catalog (Gaia Collaboration 2018; Arenou et al. 2018; Lindegren et al. 2018), with a maximum separation of $1''$. To ensure the nearby nature of the matched sources, we selected only the sources that have a parallax value larger than the parallax error. We find 10% matches that we then remove from the GC catalog. We note that we also matched our catalog of dwarf nuclei to the GC catalog in order to identify possible nuclei contamination. The histograms of the absolute magnitudes of all detected GCs in the MATLAS fields, the GCs that are *Gaia* matches and the GCs that are nuclei matches are shown in Fig. 14 (left). Unlike the *Gaia* matches, we did not remove the

nuclei matches since it is not possible to determine if the nucleus is real or is a GC projected near the galaxy center.

6.2. Background and completeness correction

In order to compute the total number of GCs associated with a traditional dwarf or a UDG, we first compute the number of GCs within $2R_e$ (a reasonable radius to select; see Müller et al. 2021), subsequently referred to as N_{GCobs} . A total of 1589 MATLAS dwarfs have a measured effective radius (Poulain et al. 2021a), including, by definition, all of our 59 UDGs. Of these, 1380 have no GC candidate within $2R_e$, 36 of which are UDGs (i.e., 209 MATLAS dwarfs have $N_{GCobs} > 0$, 23 of which are UDGs). We then applied a background correction. The number of sources per unit area was computed for the surrounding region of size 3 to $7R_e$. This number was then scaled to the circular area of radius $2R_e$ and removed from N_{GCobs} , resulting in a background corrected N_{GCobs} . The background region outer radius of $7R_e$ extends beyond the MATLAS field of view for 21 MATLAS dwarfs, including one UDG (MATLAS-1177). In this case, the background counts were corrected to account for the missing coverage. Figure 14 (right) shows the distribution of the background corrected N_{GCobs} for both the normal dwarfs (non-UDGs) and our UDGs sample with GALFIT parameters.

Finally, a completeness correction was applied by assuming a GCLF represented by a Gaussian with peak absolute magnitude $M_V = -7.6 \pm 0.1$ mag (Rejkuba 2012) and taking into account the magnitude limit of the GC catalog in each MATLAS field. A correcting factor was then applied to the background corrected N_{GCobs} based on the part of the GCLF that is fainter than the observed limit, resulting in the quantity N_{GC} . In summary, a total of 23 UDGs and 186 traditional dwarf (non-UDGs) galaxies have GALFIT parameter R_e and $N_{GC} > 0$.

6.3. Specific frequency

As the number of GCs is a function of the brightness of the host galaxy, we show in Fig. 15 (left) the computed values of N_{GC} as a function of the host galaxy absolute magnitude in the V-band M_V . The value for MATLAS-2019 is highlighted in the plot and compared to the one recently measured from HST observations and published in Müller et al. (2021). Our result based on the ground-based CFHT data is in very good agreement with the space-based HST data.

The specific frequency S_N (Harris & van den Bergh 1981) was computed using the formula:

$$S_N = N_{GC} \cdot 10^{0.4(M_V+15)} \quad (1)$$

where N_{GC} is the total, background and completeness corrected number of GCs. For MATLAS-2019, we obtain a value for N_{GC} and S_N of 26 and 63, respectively, in agreement with the value of 26 ± 6 and 58 ± 14 determined from the deep (sampling most of the GCLF) high resolution HST data (Müller et al. 2021).

Prior studies of the GC population of UDGs in the Coma and Virgo clusters (Lim et al. 2018, 2020) have claimed that the S_N of these UDGs varies dramatically, with the mean S_N being higher for UDGs than for classical dwarf (non-UDG) galaxies. Similarly, Forbes et al. (2020) finds that the richness of GCs in UDGs generally exceeds that found in normal dwarf galaxies of the same stellar mass. The specific frequencies of the MATLAS non-UDGs and UDGs are plotted in Fig. 15 (right). Considering galaxies of similar luminosity ($-15.5 < M_g < -11.5$), the GC population of the traditional dwarf (non-UDGs) galaxies and

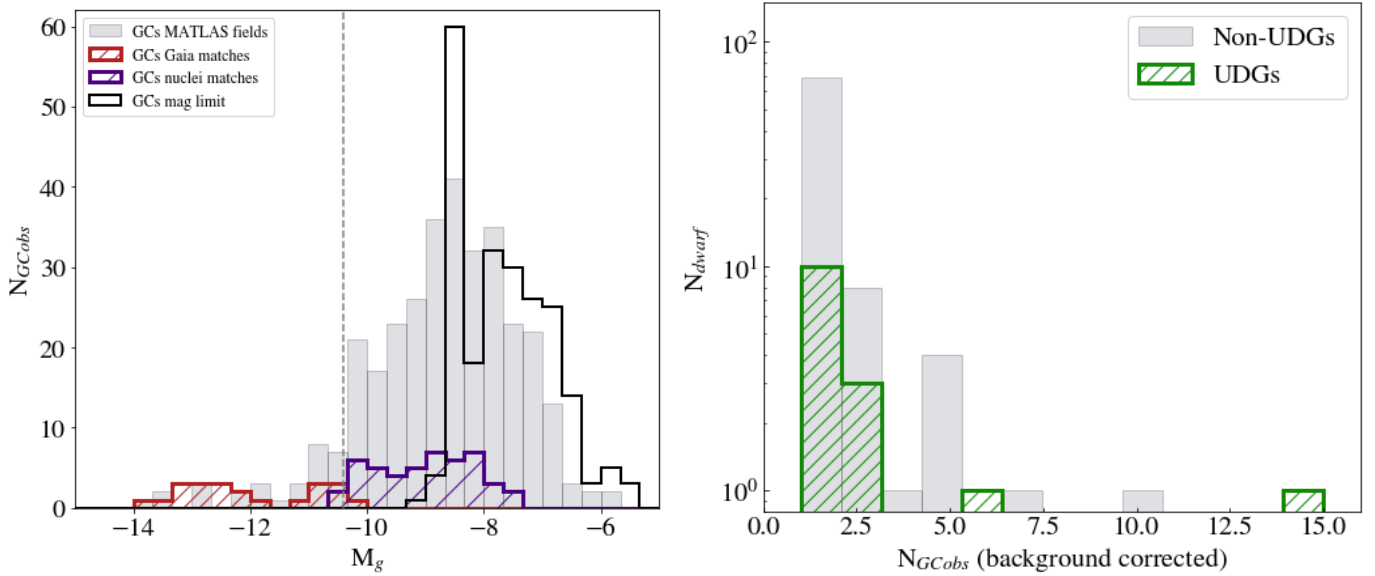


Fig. 14. *Left:* histograms of the absolute magnitudes of all detected GCs in the MATLAS fields (filled gray), the GCs that are *Gaia* matches (hashed red) and the GCs that are nuclei matches (hashed violet). The *Gaia* matches were removed from the GC sample but the nuclei matches were kept since some may be real GCs seen in projection at the center of the galaxy. The GC detection limiting absolute magnitudes for each galaxy are displayed as the black solid line histogram. The dashed gray vertical line shows the absolute magnitude of the most luminous Milky Way globular cluster, Omega Centauri ($M_V = -10.4$). *Right:* histogram of the GC counts $N_{GC,obs}$, *Gaia* matches removed and background corrected, for the MATLAS non-UDGs (filled gray) and UDGs (hashed green).

UDGs span the same range of values. At the faint end, that is, for dwarfs with $M_V \gtrsim -11.5$, we find only traditional dwarfs since the UDGs that are that faint have no valid GALFIT parameters due to their extremely low surface brightness. Hence, for dwarfs with $-15.5 \lesssim M_V \lesssim -11.5$ in low to moderate density environments, we find no evidence of a higher S_N for UDGs than for traditional dwarf (non-UDG) galaxies, contrary to what is found in most clusters.

6.4. Halo mass

The virial mass of the MATLAS UDGs can be estimated using the number of GCs in a system (Harris et al. 2013; Beasley et al. 2016). The virial mass of a galaxy scales linearly with the number of GCs over six orders of magnitude (Harris et al. 2013), the relation only flattens for halos with masses smaller than $10^{10} M_\odot$ or $N_{GC} \gtrsim 3$ (Burkert & Forbes 2020, see their Fig. 1). According to Harris et al. (2017), the virial mass M_{halo} of a galaxy is connected to the total mass of the GC system $M_{GC,tot}$ via the following formula:

$$M_{GC,tot}/M_{halo} = 2.9 \times 10^{-5} \quad (2)$$

The uncertainties associated with M_{halo} are computed from the 0.28 dex scatter of the $M_{GC,tot}-M_{halo}$ relation (Harris et al. 2017). As in Müller et al. (2021), we assume a mean mass of a GC to be $1 \times 10^5 M_\odot$ for dwarf galaxies (Harris et al. 2017) and therefore multiply that number by N_{GC} to compute $M_{GC,tot}$.

The distributions of halo masses for the 23 UDGs and 186 traditional dwarf (non-UDGs) galaxies with GALFIT parameter R_e and $N_{GC} > 0$ are shown in Fig. 16 (top). The $N_{GC} > 3$ demarcation line is shown in the figure. The halo-to-stellar mass ratio distribution can be computed for those 19 UDGs and 151 traditional dwarf (non-UDGs) galaxies with estimated stellar masses (see Sect. 5.3). As can be seen in Fig. 16 (bottom), the halo-to-stellar mass ratio distribution for the UDGs peaks at roughly the

same value as for the traditional dwarf (non-UDGs) galaxies, but spans the smaller range of $M_h/M_* \sim 10-2000$. The distribution for $N_{GC} > 3$ is also shown in the figure.

For MATLAS-2019, we measure a GC system mass of $M_{GC,tot} = 2.6 \pm 0.6 \times 10^6 M_\odot$ and a halo mass of $M_{halo} = 0.9 \pm 0.2 \times 10^{11} M_\odot$. A table of these derived properties of the MATLAS UDGs can be found in Appendix C.

7. Tidal features in UDGs

One of the possible scenarios for UDG formation is that they are formed via tidal disruption (Carleton et al. 2019; Román et al. 2021; Gannon et al. 2021). Another scenario is that some UDGs could be Tidal Dwarf Galaxies (TDGs), that is galaxies formed from gas expelled from a massive galaxy after an interaction. Therefore, searching for tidal features, the remnants of gravitational interactions between galaxies (Bílek et al. 2020), can be a powerful tool in constraining the formation scenario of UDGs.

A search for tidal features in dwarfs in the Local Universe was presented by Paudel et al. (2018). They visually identified tidal features and classified them in two main categories, dwarf-dwarf interaction/merger and dwarf-giant interactions, with a further grouping of their tidal features into three categories: interacting (ongoing interaction between two dwarf galaxies), shell (presence of shell features) and tidal tail (presence of amorphous tidal features such as tidal streams or plumes which cannot be placed into the other classifications). Shell features in dwarfs can be produced by a merger origin (Paudel et al. 2017) whereas an S-shaped elongated stellar envelope is likely due to tidal stretching from a nearby giant galaxy (Paudel et al. 2013; Paudel & Ree 2014). Another nice example of a candidate UDG with an S-shape is the LSB dwarf HCC-087 in the Hydra I cluster (Koch et al. 2012), whose photometric properties are given in the works of Misgeld et al. (2008) and Misgeld & Hilker (2011).

In our visual inspection of the UDGs, we follow the same classification scheme. We visually inspected both the g -band

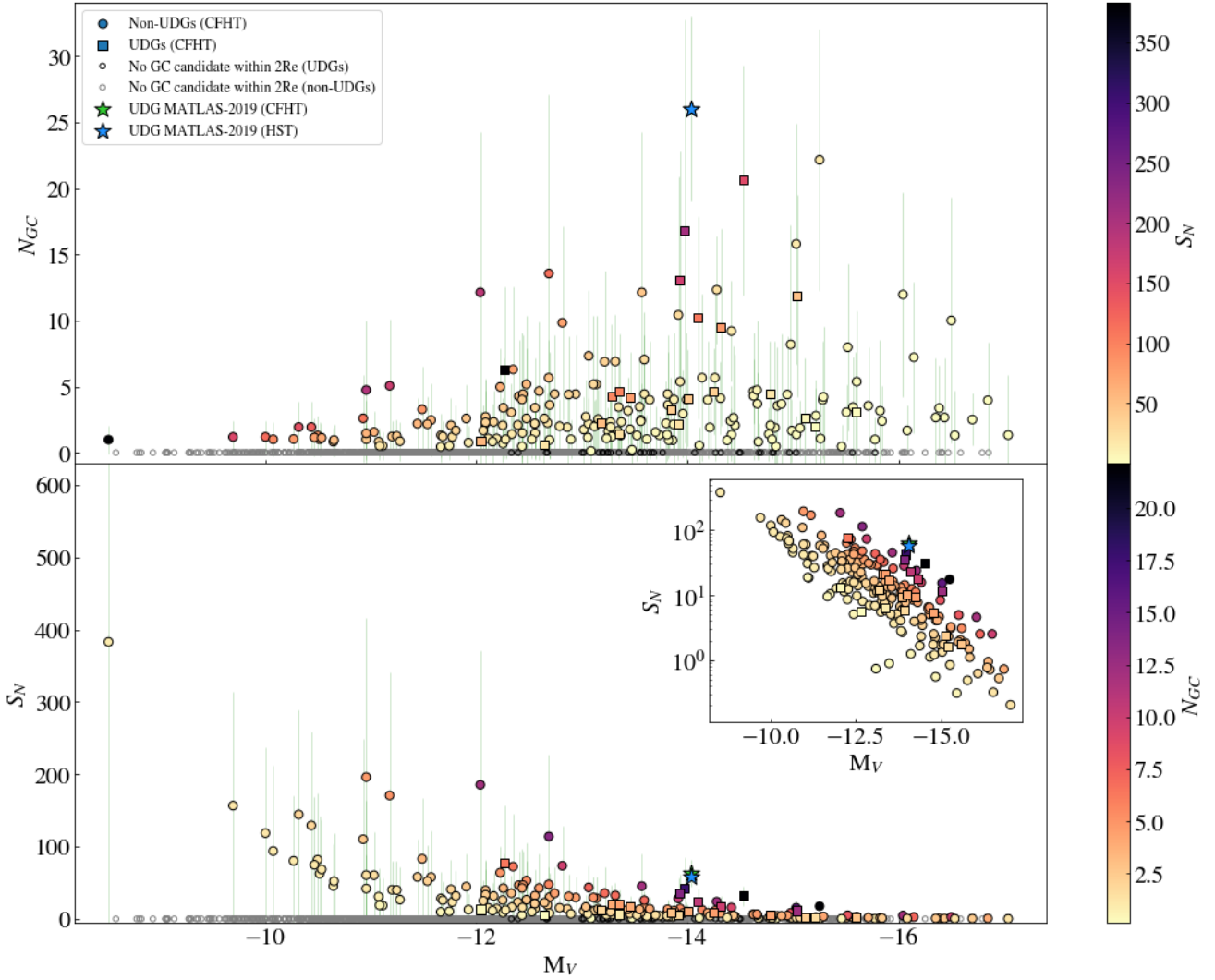


Fig. 15. *Top:* background and completeness corrected N_{GC} as a function of absolute magnitude for the 23 UDGs (squares) and 186 traditional dwarf (non-UDGs) galaxies (circles) with $N_{GC} > 0$. The color bar indicates the value of the specific frequency S_N . The UDG MATLAS-2019 observed with HST (Müller et al. 2021) is shown with the star symbol. *Bottom:* same as top but now showing the specific frequency S_N in the plot and the background and completeness corrected N_{GC} in the color bar. The inset plot is with y-axis in log scale. In both plots, the 36 UDGs (black open circles) and 1344 non-UDGs (gray open circles) with a measured GALFIT effective radius and no GC candidate within $2R_e$ are shown. In total, 1380 out of the 1589 MATLAS dwarfs with a measured GALFIT effective radius have no GC candidate within $2R_e$.

and color images of the MATLAS UDGs and found that five out of the 59 MATLAS UDGs (MATLAS-262, MATLAS-951, MATLAS-1059, MATLAS-1779 and MATLAS-1615) show signs of tidal disruptions. As can be seen in Fig. 17, all cases are dwarf-giant interactions and exhibit low surface brightness features extending in the direction of one or more massive galaxies (central ETG in the field: NGC 1248, NGC 3640, NGC 3674, NGC 5493 and NGC 5355, respectively). In particular, 1) MATLAS-262 is observed as a condensation within a long stream, oriented in the east-west direction, and appears to be close to perpendicular to a putative host edge-on galaxy; the other filamentary structure close to the UDG with a NW-SE orientation is likely a foreground cirrus as several other such structures with the same orientation are seen in the field; 2) MATLAS-951 has streams with a clear S-shape; 3) MATLAS-1059 shows small tidal extensions; 4) MATLAS-1779 has streams with a possible S-shape, however, there is contamination by a ghost stellar halo; and 5) MATLAS-1615 displays streams oriented in the SE-NW direction, but is

located in a high background region caused by ghost stellar halos.

Another two UDGs (MATLAS-368 and MATLAS-2184) were found to show extended asymmetric isophotes (central ETG in the field: NGC 2577 and NGC 7454, respectively). However, MATLAS-2184 is in a region with many cirrus so the asymmetric extension is possibly due to cirrus contamination. Optical cirrus exhibit on the CFHT images a range of colors (see Miville-Deschênes et al. 2016), and some have very similar colors as the stellar structures (Sola et al., in prep.). Thus using colors in the optical regime is not enough to separate cirrus from tidal features. Having a broader range of wavelengths (from the ultraviolet to the infrared), may be tested, but data still lack to do such an experiment. In the near future, combining GALEX, Euclid and WISE data might be useful for that purpose.

For two of the UDGs (MATLAS-478 and MATLAS-1824), no tidal features associated with the dwarf were seen but they were found to be located at the end of the tidal tail of the nearby massive (host) galaxy (NGC 2768 and NGC 5557, respectively).

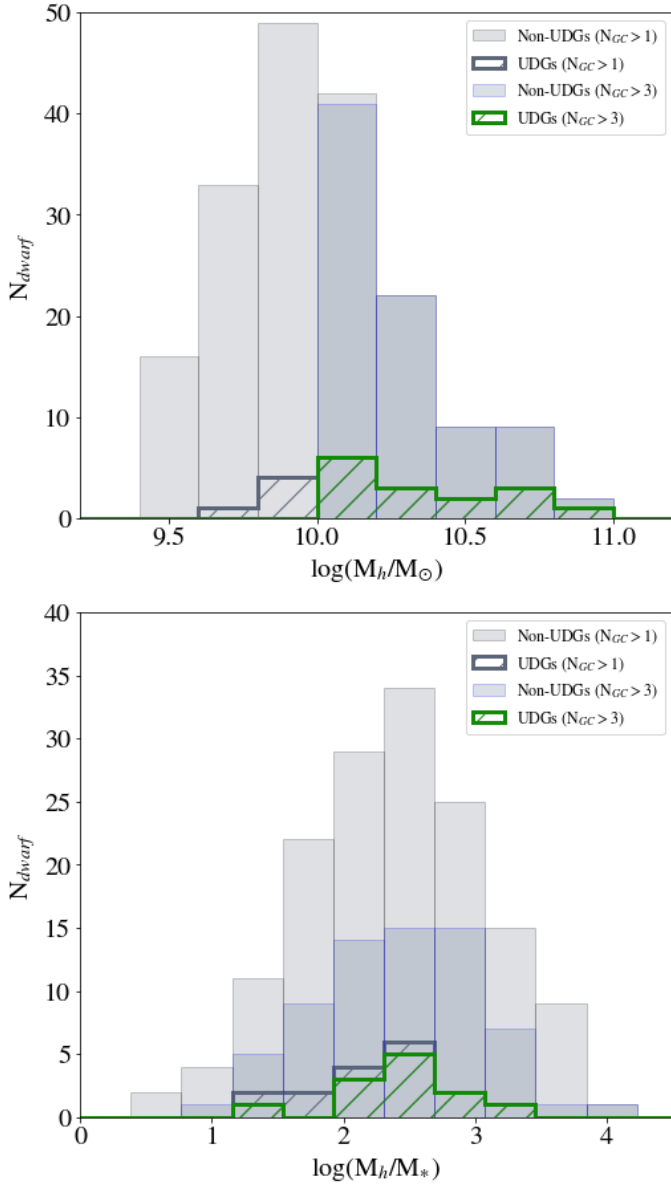


Fig. 16. *Top:* distributions of halo masses for the 20 UDGs (hashed green) and 162 traditional dwarf (non-UDGs) galaxies (filled gray) with GALFIT parameter R_e and $N_{GC} > 1$. The hashed green (15 UDGs) and filled blue (68 non-UDGs) histograms are for the galaxies with $N_{GC} > 3$. *Bottom:* distributions of halo-to-stellar mass ratios for the 17 UDGs (hashed gray) and 135 traditional dwarf (non-UDGs) galaxies (filled gray) with GALFIT parameter R_e and $N_{GC} > 1$ and stellar masses. The hashed green (12 UDGs) and filled blue (56 non-UDGs) histograms are for the galaxies with $N_{GC} > 3$ and stellar masses.

MATLAS-478, is nucleated (dE,N), and a TDG candidate: the host galaxy is strongly disrupted and the tail emanates from the host in the direction of the UDG. MATLAS-1824 is a spectroscopically confirmed TDG (Duc et al. 2014).

Although the majority of the MATLAS UDGs do not appear to show evidence of recent tidal disruption or having formed as a TDG, one should note that we are able to recognize tidally disrupted dwarfs and TDGs only for a limited amount of time as tails of giant ellipticals live for only about 0.5 Gyr (Mancillas et al. 2019) and the orbital time of a star 10 kpc away from a 10 billion solar masses galaxy is only 1 Gyr. Therefore a UDG that would be tidally perturbed 10 Gyr ago ($z \sim 2$),

when galaxy interactions were common, would most likely look relaxed today. We note that the majority (5/7) of the UDGs with tidal features or asymmetric isophotes are nucleated (dE,N), and do not show any difference in color than the other UDGs.

We now examine the local environment in which these UDGs, tidally disrupted dwarfs and TDGs, are found. One might expect the UDGs with tidal features to be located in more dense environments where they are more likely to have interactions. However, we find them in a range of environments. As seen in Fig. 3, the five UDGs that show signs of tidal disruptions are found at both low and high ρ_{10} values. The two UDGs that are TDGs are located at similar, moderately low ρ_{10} values, but this may be an observational bias; if the system is in a higher density environment, the tidal tail may not be as long lived.

The individual systems where the tidally disrupted UDGs are located, shown in the maps in Appendix B, further illustrate the diverse environments in which these galaxies are found. Some are projected to lie within the virial radii of various groups (e.g., NGC 3685, NGC 3640, NGC 2530), while other are not within any of the Kourkchi & Tully optically identified groups (e.g., NGC 5493, NGC 1248). Some of these UDGs are located near galaxies with signatures of old major mergers (e.g., NGC 5493), while at least one is in close projection to a massive galaxy that has undergone a recent major merger (e.g., NGC 3641). The two TDG UDGs are both outside of the optically identified groups, although one is just outside the estimated boundary, such that the host ETG is considered a group member.

Here we have only considered the impact of the massive galaxies on the UDGs, but tidal features can also be caused by dwarf-dwarf interactions. A full analysis of the tidal features in the larger MATLAS dwarf sample is ongoing.

8. HI in UDGs

The detection of HI in a UDG allows us to not only measure its HI gas content but also to directly obtain a radial velocity and hence a distance estimate for the UDG. In the particular case of the MATLAS UDGs, this is an important tool given the uncertainties associated with assuming that the UDG is at the distance of the central massive ETG (presumed host). Past studies of HI-bearing UDGs located in the field (Leisman et al. 2017), groups (Spekkens & Karunakaran 2018) and poor galaxy clusters (Shi et al. 2017) have reported bluer colors, narrower line widths, larger gas fractions as compared to galaxies of similar HI-mass and environment.

We examined how many of the MATLAS UDGs are located in the regions observed for the ALFALFA and ATLAS^{3D} HI surveys. As mentioned in Sect. 3.1, of the 51 UDGs located in the observed regions, only three have a HI line detection (MATLAS-42, MATLAS-1337 in the ALFALFA catalog and MATLAS-1824 in our WRST catalog). These galaxies are located at HI distances of 33.5, 36 and 46.3 Mpc with HI masses $8.0 \leq \log(M_{HI}) \leq 8.3$ (Poulain et al. 2021a). Based on the number of galaxies located in the observed regions and considering stellar masses high enough so we might detect HI (see Poulain et al. 2021a), we estimate a frequency of HI-bearing UDGs lower than for traditional dwarfs with $\sim 7\%$ and $\sim 10\%$, respectively.

In Poulain et al. (2021a), we compare the properties of these HI UDGs with those of traditional dwarf (non-UDGs) galaxies of similar HI mass. We find that the UDGs line widths are smaller than the median line width of the HI traditional dwarfs. Only two of the three HI UDGs have an available observation in the r - and i -band and thus an estimated stellar mass. Only one of these two HI UDGs has a gas fraction larger than the median of

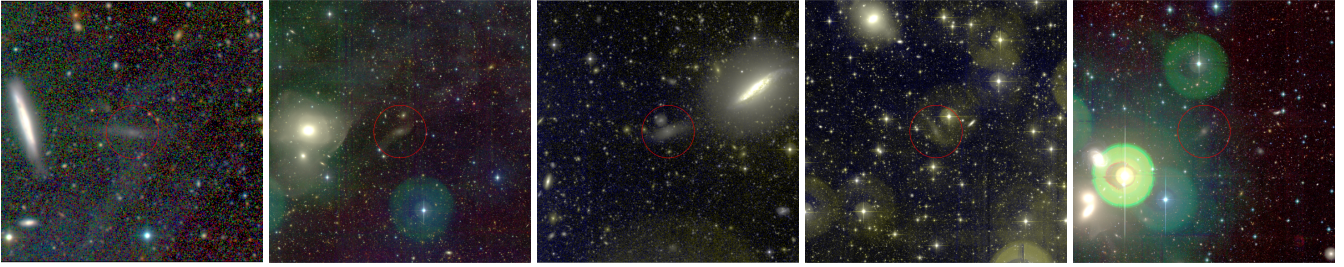


Fig. 17. Color (g, r, i) images of the five UDGs that show signs of tidal disruption (from left to right: MATLAS-262, MATLAS-951, MATLAS-1059, MATLAS-1779 and MATLAS-1615). They show, from left to right: MATLAS-262 as a condensation within a long stream oriented in the east-west direction, close to perpendicular to an edge-on galaxy; the other filamentary structure close to the UDG with a NW-SE orientation is likely a foreground cirrus; MATLAS-951 has streams with a clear S-shape; MATLAS-1059 shows small tidal extensions; MATLAS-1779 has streams with a possible S-shape but there is contamination by a ghost stellar halo; and MATLAS-1615 displays streams oriented in the SE-NW direction but located in a high background region caused by multiple ghost stellar halos. From left to right, the image is 3, 25, 8, 25 and 25 sq.arcmin. in size. North is up and east is left.

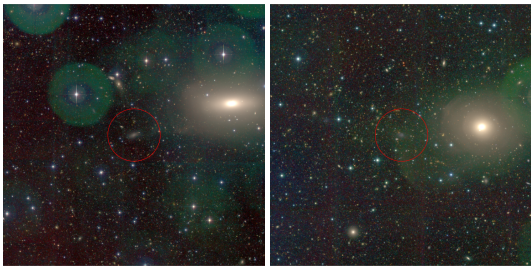


Fig. 18. Images of the two UDGs that are TDG candidates from left to right: MATLAS-478 and MATLAS-1824). They are found at the end of the tidal tail of a nearby massive galaxy, visible on the right in the image. From left to right, the image is 20 and 25 sq.arcmin. in size. North is up and east is left.

the traditional dwarf distribution and bluer colors than the traditional dwarfs of similar HI mass, the other one having redder colors than the median colors. We note that, given the low number statistics, the observed properties might not represent the overall HI-bearing UDG population.

One of the three HI UDGs, MATLAS-1824, is located along a prominent tidal tail of the massive galaxy NGC 5557, already mentioned in Sect. 7. This UDG is also part of the six TDGs around ATLAS^{3D} ETGs showing fine structures identified by Duc et al. (2014), two of them having UDG properties based on their light profile fitting (see their Table 3). Another elongated tidal feature, perpendicular to the shell, passes through MATLAS-1824 and connects to another HI UDG, MATLAS-1830, which is not in our UDG sample due to the absence of successful two-dimensional surface brightness modeling caused by its extremely low surface brightness.

9. Conclusions

We have identified a population of UDGs in the MATLAS fields. Assuming the distance to the central ETG in the field and using the known distances when available, 59 UDGs were robustly identified using a two-dimensional surface brightness Sérsic profile fit and a cut in surface brightness and effective radius. We find that they are at distances of 19.1–46.3 Mpc and located predominantly in groups, with 32% of the UDGs in groups with observed X-ray emission and 61% within the estimated virial radii of optically identified groups detected via a galaxy linkage algorithm by Kourkchi & Tully (2017). The X-ray groups are all contained within the Kourkchi & Tully (2017) catalog. Most of

the X-ray groups have been well studied in the literature, and UDGs are associated with both dynamically young and dynamically relaxed systems.

Based on a detailed analysis of their photometric and structural properties, we find that the MATLAS UDGs do not belong to a separate and distinct group but instead are an extension to the traditional dwarf galaxies, making a clear-cut delineation/definition for a UDG arbitrary. The majority of the MATLAS UDGs are visually classified morphologically as dwarf ellipticals with log stellar masses in the range ~ 6.5 – 8.7 . The fraction of nucleated UDGs ($\sim 34\%$) is slightly above the one measured for all MATLAS dwarfs (visual: $\sim 23\%$, GALFIT: $\sim 27\%$). However, looking at the dwarfs with M_g in the range of the UDGs luminosity (-15.5 to -11.5), the nucleated fraction of the traditional dwarf (non-UDG) galaxies is $\sim 34\%$, similar to the nucleated fraction of the UDGs. The MATLAS UDGs exhibit the same wide range of colors as the traditional dwarf galaxies, with $(g-r)_0 = -0.1$ to 0.8 and $(g-i)_0 = -0.2$ to 1.2 . Their median color, $(g-r)_0 = 0.36$, is as red as the one measured in galaxy clusters such as Coma, $(g-r)_0 = 0.40$, but the range of colors is narrower.

Only five ($\sim 8\%$) UDGs show signs of tidal disruptions and only two are tidal dwarf galaxy candidates. Although the majority of the MATLAS UDGs do not appear to show evidence of recent tidal disruption or having formed as a TDG, one should note that we are able to recognize tidally disrupted dwarfs and TDGs only for a limited amount of time. A UDG that would be tidally perturbed 10 Gyr ago ($z \sim 2$), for example, would most likely look relaxed today. Three MATLAS UDGs are detected in HI, two in the ALFALFA catalog and one in our WRST catalog. One of these, MATLAS-1824, is a spectroscopically confirmed TDG located along a prominent tail of the massive galaxy NGC 5557. A study of globular cluster candidates selected in the CFHT multiband images finds, for the range of magnitude $-15.5 \lesssim M_V \lesssim -11.5$, no evidence of a higher GC specific frequency S_N for UDGs than for traditional dwarf (non-UDG) galaxies, contrary to what is found in most clusters. The UDGs halo-to-stellar mass ratio distribution, as estimated from the GC count, peaks at roughly the same value as for the traditional dwarf (non-UDGs) galaxies, but spans the smaller range of $M_h/M_* \sim 10$ – 2000 . We interpret these results to mean that the large majority of the field-to-group UDGs do not have a different formation scenario than traditional dwarf galaxies.

Acknowledgements. The authors would like to thank the referee for his/her thoughtful comments, which helped improve the work. This research is based

on observations obtained with MegaPrime/MegaCam, a joint project of CFHT and CEA/IRFU, at the Canada-France-Hawaii Telescope (CFHT) which is operated by the National Research Council (NRC) of Canada, the Institut National des Sciences de l'Univers of the Centre National de la Recherche Scientifique (CNRS) of France, and the University of Hawaii. This work is based in part on data products produced at Terapix available at the Canadian Astronomy Data Centre as part of the Canada-France-Hawaii Telescope Legacy Survey, a collaborative project of NRC and CNRS. M. P. acknowledges the Vice Rector for Research of the University of Innsbruck for the granted scholarship. S. P. acknowledges support from the New Researcher Program (Shinjin grant No. 2019R1C1C1009600) through the National Research Foundation of Korea. S. L. acknowledges the support from the Sejong Science Fellowship Program through the National Research Foundation of Korea (NRF-2021R1C1C2006790). M. B. acknowledges the support from the Polish National Science Centre under the grant 2017/26/D/ST9/00449. This work has made use of data from the European Space Agency (ESA) mission *Gaia* (<https://www.cosmos.esa.int/gaia>), processed by the *Gaia* Data Processing and Analysis Consortium (DPAC, <https://www.cosmos.esa.int/web/gaia/dpac/consortium>). Funding for the DPAC has been provided by national institutions, in particular the institutions participating in the *Gaia* Multilateral Agreement. Funding for the Sloan Digital Sky Survey IV has been provided by the Alfred P. Sloan Foundation, the US Department of Energy Office of Science, and the Participating Institutions. SDSS-IV acknowledges support and resources from the Center for High Performance Computing at the University of Utah. The SDSS website is www.sdss.org. SDSS-IV is managed by the Astrophysical Research Consortium for the Participating Institutions of the SDSS Collaboration including the Brazilian Participation Group, the Carnegie Institution for Science, Carnegie Mellon University, Center for Astrophysics Harvard & Smithsonian, the Chilean Participation Group, the French Participation Group, Instituto de Astrofísica de Canarias, The Johns Hopkins University, Kavli Institute for the Physics and Mathematics of the Universe (IPMU)/University of Tokyo, the Korean Participation Group, Lawrence Berkeley National Laboratory, Leibniz Institut für Astrophysik Potsdam (AIP), Max-Planck-Institut für Astronomie (MPIA Heidelberg), Max-Planck-Institut für Astrophysik (MPA Garching), Max-Planck-Institut für Extraterrestrische Physik (MPE), National Astronomical Observatories of China, New Mexico State University, New York University, University of Notre Dame, Observatório Nacional/MCTI, The Ohio State University, Pennsylvania State University, Shanghai Astronomical Observatory, United Kingdom Participation Group, Universidad Nacional Autónoma de México, University of Arizona, University of Colorado Boulder, University of Oxford, University of Portsmouth, University of Utah, University of Virginia, University of Washington, University of Wisconsin, Vanderbilt University, and Yale University.

References

- Afanasiev, V. L., & Silchenko, O. K. 2007, *Astron. Astrophys. Trans.*, **26**, 311
- Aguerrí, J. A. L., Castro-Rodríguez, N., Napolitano, N., Arnaboldi, M., & Gerhard, O. 2006, *A&A*, **457**, 771
- Alabi, A. B., Forbes, D. A., Romanowsky, A. J., et al. 2016, *MNRAS*, **460**, 3838
- Albaret, F. D., Allende Prieto, C., Almeida, A., et al. 2017, *ApJS*, **233**, 25
- Amorisco, N. C., & Loeb, A. 2016, *MNRAS*, **459**, L51
- Ann, H. B., Seo, M., & Ha, D. K. 2015, *ApJS*, **217**, 27
- Arenou, F., Luri, X., Babusiaux, C., et al. 2018, *A&A*, **616**, A17
- Barbosa, C. E., Zaritsky, D., Donnerstein, R., et al. 2020, *ApJS*, **247**, 46
- Beasley, M. A., Romanowsky, A. J., Pota, V., et al. 2016, *ApJ*, **819**, L20
- Behroozi, P. S., Wechsler, R. H., & Conroy, C. 2013, *ApJ*, **770**, 57
- Bell, E. F., McIntosh, D. H., Katz, N., & Weinberg, M. D. 2003, *ApJS*, **149**, 289
- Benavides, J. A., Sales, L. V., Abadi, M. G., et al. 2021, *Nat. Astron.*, in press, [[arXiv:2109.01677](https://arxiv.org/abs/2109.01677)]
- Bennet, P., Sand, D. J., Crnojević, D., et al. 2017, *ApJ*, **850**, 109
- Bertin, E., & Arnouts, S. 1996, *A&AS*, **117**, 393
- Bílek, M., Duc, P.-A., Cuillandre, J.-C., et al. 2020, *MNRAS*, **498**, 2138
- Binggeli, B., Sandage, A., & Tammann, G. A. 1985, *AJ*, **90**, 1681
- Blakeslee, J. P. 1999, *AJ*, **118**, 1506
- Blakeslee, J. P., & Cantiello, M. 2018, *Res. Notes Am. Astron. Soc.*, **2**, 146
- Blanton, M. R., Bershady, M. A., Abolfathi, B., et al. 2017, *AJ*, **154**, 28
- Bogdán, Á. 2020, *ApJ*, **901**, L30
- Brough, S., Forbes, D. A., Kilborn, V. A., & Couch, W. 2006, *MNRAS*, **370**, 1223
- Burkert, A., & Forbes, D. A. 2020, *AJ*, **159**, 56
- Cappellari, M., Emsellem, E., Krajnović, D., et al. 2011a, *MNRAS*, **413**, 813
- Cappellari, M., Emsellem, E., Krajnović, D., et al. 2011b, *MNRAS*, **416**, 1680
- Carleton, T., Errani, R., Cooper, M., et al. 2019, *MNRAS*, **485**, 382
- Carlsten, S. G., Greco, J. P., Beaton, R. L., & Greene, J. E. 2020, *ApJ*, **891**, 144
- Chiboucas, K., Jacobs, B. A., Tully, R. B., & Karachentsev, I. D. 2013, *AJ*, **146**, 126
- Crnojević, D., Sand, D. J., Caldwell, N., et al. 2014, *ApJ*, **795**, L35
- Dalcanton, J. J., Spergel, D. N., Gunn, J. E., Schmidt, M., & Schneider, D. P. 1997, *AJ*, **114**, 635
- Danieli, S., van Dokkum, P., Conroy, C., Abraham, R., & Romanowsky, A. J. 2019, *ApJ*, **874**, L12
- Di Cintio, A., Brook, C. B., Dutton, A. A., et al. 2017, *MNRAS*, **466**, L1
- Doppel, J. E., Sales, L. V., Navarro, J. F., et al. 2021, *MNRAS*, **502**, 1661
- Du, W., Wu, H., Lam, M. I., et al. 2015, *AJ*, **149**, 199
- Duc, P. A. 2020, *ArXiv e-prints* [[arXiv:2007.13874](https://arxiv.org/abs/2007.13874)]
- Duc, P.-A., Paudel, S., McDermid, R. M., et al. 2014, *MNRAS*, **440**, 1458
- Duc, P.-A., Cuillandre, J.-C., Karabal, E., et al. 2015, *MNRAS*, **446**, 120
- Durrell, P. R., Côté, P., Peng, E. W., et al. 2014, *ApJ*, **794**, 103
- Eigenthaler, P., & Zeilinger, W. W. 2010, *A&A*, **511**, A12
- Eigenthaler, P., Puzia, T. H., Taylor, M. A., et al. 2018, *ApJ*, **855**, 142
- Emsellem, E., van der Burg, R. F. J., Fensch, J., et al. 2019, *A&A*, **625**, A76
- Fensch, J., van der Burg, R. F. J., Jeřábková, T., et al. 2019a, *A&A*, **625**, A77
- Fensch, J., Duc, P.-A., Boquien, M., et al. 2019b, *A&A*, **628**, A60
- Ferrarese, L., Côté, P., Cuillandre, J., et al. 2012, *ApJS*, **200**, 4
- Ferrarese, L., Côté, P., MacArthur, L. A., et al. 2020, *ApJ*, **890**, 128
- Finoguenov, A., Davis, D. S., Zimer, M., & Mulchaey, J. S. 2006, *ApJ*, **646**, 143
- For, B. Q., Staveley-Smith, L., Westmeier, T., et al. 2019, *MNRAS*, **489**, 5723
- Forbes, D. A., Alabi, A., Brodie, J. P., et al. 2017, *AJ*, **153**, 114
- Forbes, D. A., Gannon, J., Couch, W. J., et al. 2019, *A&A*, **626**, A66
- Forbes, D. A., Alabi, A., Romanowsky, A. J., Brodie, J. P., & Arimoto, N. 2020, *MNRAS*, **492**, 4874
- Forbes, D. A., Gannon, J. S., Romanowsky, A. J., et al. 2021, *MNRAS*, **500**, 1279
- Gaia Collaboration (Brown, A. G. A., et al.) 2018, *A&A*, **616**, A1
- Gannon, J. S., Dullo, B. T., Forbes, D. A., et al. 2021, *MNRAS*, **502**, 3144
- Georgiev, I. Y., Puzia, T. H., Goudfrooij, P., & Hilker, M. 2010, *MNRAS*, **406**, 1967
- Giuricin, G., Marinoni, C., Ceriani, L., & Pisani, A. 2000, *ApJ*, **543**, 178
- Graham, A. W., & Driver, S. P. 2005, *PASA*, **22**, 118
- Greco, J. P., Greene, J. E., Strauss, M. A., et al. 2018, *ApJ*, **857**, 104
- Gu, M., Conroy, C., Law, D., et al. 2018, *ApJ*, **859**, 37
- Habas, R., Marleau, F. R., Duc, P.-A., et al. 2020, *MNRAS*, **491**, 1901
- Harris, W. E., & van den Bergh, S. 1981, *AJ*, **86**, 1627
- Harris, W. E., Harris, G. L. H., & Alessi, M. 2013, *ApJ*, **772**, 82
- Harris, W. E., Blakeslee, J. P., & Harris, G. L. H. 2017, *ApJ*, **836**, 67
- Haynes, M. P., Giovanelli, R., Kent, B. R., et al. 2018, *ApJ*, **861**, 49
- Heesters, N., Habas, R., Marleau, F. R., et al. 2021, *A&A*, in press, [<https://doi.org/10.1051/0004-6361/202141184>]
- Helsdon, S. F., & Ponman, T. J. 2003, *MNRAS*, **340**, 485
- Helsdon, S. F., Ponman, T. J., & Mulchaey, J. S. 2005, *ApJ*, **618**, 679
- Hudson, M. J., Harris, G. L., & Harris, W. E. 2014, *ApJ*, **787**, L5
- Impey, C., Bothun, G., & Malin, D. 1988, *ApJ*, **330**, 634
- Iodice, E., Cantiello, M., Hilker, M., et al. 2020, *A&A*, **642**, A48
- Janssens, S. R., Abraham, R., Brodie, J., Forbes, D. A., & Romanowsky, A. J. 2019, *ApJ*, **887**, 92
- Kadowaki, J., Zaritsky, D., & Donnerstein, R. L. 2017, *ApJ*, **838**, L21
- Karachentsev, I. D., Makarov, D. I., & Kaisina, E. I. 2013, *AJ*, **145**, 101
- Koch, A., Burkert, A., Rich, R. M., et al. 2012, *ApJ*, **755**, L13
- Koda, J., Yagi, M., Yamanoi, H., & Komiyama, Y. 2015, *ApJ*, **807**, L2
- Kourkchi, E., & Tully, R. B. 2017, *ApJ*, **843**, 16
- Kovács, O. E., Bogdán, Á., & Canning, R. E. A. 2019, *ApJ*, **879**, L12
- Lee, J. H., Kang, J., Lee, M. G., & Jang, I. S. 2020, *ApJ*, **894**, 75
- Leisman, L., Haynes, M. P., Janowiecki, S., et al. 2017, *ApJ*, **842**, 133
- Lelli, F., Duc, P.-A., Brinks, E., et al. 2015, *A&A*, **584**, A113
- Lim, S., Peng, E. W., Duc, P.-A., et al. 2017, *ApJ*, **835**, 123
- Lim, S., Peng, E. W., Côté, P., et al. 2018, *ApJ*, **862**, 82
- Lim, S., Côté, P., Peng, E. W., et al. 2020, *ApJ*, **899**, 69
- Lindgren, L., Hernández, J., Bombrun, A., et al. 2018, *A&A*, **616**, A2
- Mahdavi, A., Trentham, N., & Tully, R. B. 2005, *AJ*, **130**, 1502
- Mancera Piña, P. E., Aguerrí, J. A. L., Peletier, R. F., et al. 2019, *MNRAS*, **485**, 1036
- Mancillas, B., Duc, P.-A., Combes, F., et al. 2019, *A&A*, **632**, A122
- Martínez-Delgado, D., Läsker, R., Sharina, M., et al. 2016, *AJ*, **151**, 96
- McConnachie, A. W. 2012, *AJ*, **144**, 4
- McConnachie, A. W., Huxor, A., Martin, N. F., et al. 2008, *ApJ*, **688**, 1009
- Merritt, A., van Dokkum, P., Danieli, S., et al. 2016, *ApJ*, **833**, 168
- Mihos, J. C., Durrell, P. R., Ferrarese, L., et al. 2015, *ApJ*, **809**, L21
- Misgeld, I., & Hilker, M. 2011, *MNRAS*, **414**, 3699
- Misgeld, I., Mieske, S., & Hilker, M. 2008, *A&A*, **486**, 697
- Miville-Deschênes, M. A., Duc, P. A., Marleau, F., et al. 2016, *A&A*, **593**, A4
- Mulchaey, J. S., Davis, D. S., Mushotzky, R. F., & Burstein, D. 2003, *ApJS*, **145**, 39
- Müller, O., Jerjen, H., & Binggeli, B. 2018a, *A&A*, **615**, A105
- Müller, O., Pawłowski, M. S., Jerjen, H., & Lelli, F. 2018b, *Science*, **359**, 534

- Müller, O., Rejkuba, M., Pawłowski, M. S., et al. 2019, *A&A*, **629**, A18
- Müller, O., Marleau, F. R., Duc, P.-A., et al. 2020, *A&A*, **640**, A106
- Müller, O., Durrell, P. R., Marleau, F. R., et al. 2021, *ApJ*, submitted [arXiv:2101.10659]
- Muñoz, R. P., Puzia, T. H., Lançon, A., et al. 2014, *ApJS*, **210**, 4
- Muñoz, R. P., Eigenthaler, P., Puzia, T. H., et al. 2015, *ApJ*, **813**, L15
- Osmond, J. P. F., & Ponman, T. J. 2004, *MNRAS*, **350**, 1511
- O’Sullivan, E., Worrall, D. M., Birkinshaw, M., et al. 2011, *MNRAS*, **416**, 2916
- O’Sullivan, E., Ponman, T. J., Kolokythas, K., et al. 2017, *MNRAS*, **472**, 1482
- Paudel, S., & Ree, C. H. 2014, *ApJ*, **796**, L14
- Paudel, S., Duc, P.-A., Côté, P., et al. 2013, *ApJ*, **767**, 133
- Paudel, S., Smith, R., Duc, P.-A., et al. 2017, *ApJ*, **834**, 66
- Paudel, S., Smith, R., Yoon, S. J., Calderón-Castillo, P., & Duc, P.-A. 2018, *ApJS*, **237**, 36
- Peng, C. Y., Ho, L. C., Impey, C. D., & Rix, H.-W. 2002, *AJ*, **124**, 266
- Peng, C. Y., Ho, L. C., Impey, C. D., & Rix, H.-W. 2010, *AJ*, **139**, 2097
- Poulain, M., Marleau, F. R., Habas, R., et al. 2021a, *MNRAS*, submitted
- Poulain, M., Marleau, F. R., Habas, R., et al. 2021b, *MNRAS*, **506**, 5494
- Prole, D. J., Hilker, M., van der Burg, R. F. J., et al. 2019a, *MNRAS*, **484**, 4865
- Prole, D. J., van der Burg, R. F. J., Hilker, M., & Davies, J. I. 2019b, *MNRAS*, **488**, 2143
- Rejkuba, M. 2012, *Ap&SS*, **341**, 195
- Roberts, S., Davies, J., Sabatini, S., Auld, R., & Smith, R. 2007, *MNRAS*, **379**, 1053
- Román, J., & Trujillo, I. 2017a, *MNRAS*, **468**, 703
- Román, J., & Trujillo, I. 2017b, *MNRAS*, **468**, 4039
- Román, J., Beasley, M. A., Ruiz-Lara, T., & Valls-Gabaud, D. 2019, *MNRAS*, **486**, 823
- Román, J., Jones, M. G., Montes, M., et al. 2021, *A&A*, **649**, L14
- Sánchez-Janssen, R., Côté, P., Ferrarese, L., et al. 2019, *ApJ*, **878**, 18
- Sandage, A., & Binggeli, B. 1984, *AJ*, **89**, 919
- Schlafly, E. F., & Finkbeiner, D. P. 2011, *ApJ*, **737**, 103
- Schombert, J. M., & Bothun, G. D. 1988, *AJ*, **95**, 1389
- Schwartzberg, J. M., Phillipps, S., Smith, R. M., Couch, W. J., & Boyle, B. J. 1995, *MNRAS*, **275**, 121
- Serra, P., Oosterloo, T., Morganti, R., et al. 2012, *MNRAS*, **422**, 1835
- Shen, Z., Danieli, S., van Dokkum, P., et al. 2021, *ApJ*, **914**, L12
- Shi, D. D., Zheng, X. Z., Zhao, H. B., et al. 2017, *ApJ*, **846**, 26
- Smith Castelli, A. V., Faifer, F. R., & Escudero, C. G. 2016, *A&A*, **596**, A23
- Spekkens, K., & Karunakaran, A. 2018, *ApJ*, **855**, 28
- Spitler, L. R., & Forbes, D. A. 2009, *MNRAS*, **392**, L1
- Sprayberry, D., Impey, C. D., Irwin, M. J., & Bothun, G. D. 1997, *ApJ*, **482**, 104
- Toloba, E., Lim, S., Peng, E., et al. 2018, *ApJ*, **856**, L31
- Trujillo, I., Beasley, M. A., Borlaff, A., et al. 2019, *MNRAS*, **486**, 1192
- van der Burg, R. F. J., Muzzin, A., & Hoekstra, H. 2016, *A&A*, **590**, A20
- van der Burg, R. F. J., Hoekstra, H., Muzzin, A., et al. 2017, *A&A*, **607**, A79
- van der Marel, R. P. 2006, in *The Local Group as an Astrophysical Laboratory*, eds. M. Livio, & T. M. Brown, 17, 47
- van Dokkum, P. G., Abraham, R., Merritt, A., et al. 2015, *ApJ*, **798**, L45
- van Dokkum, P., Abraham, R., Brodie, J., et al. 2016, *ApJ*, **828**, L6
- van Dokkum, P., Cohen, Y., Danieli, S., et al. 2018a, *ApJ*, **856**, L30
- van Dokkum, P., Danieli, S., Cohen, Y., et al. 2018b, *Nature*, **555**, 629
- van Dokkum, P., Danieli, S., Abraham, R., Conroy, C., & Romanowsky, A. J. 2019, *ApJ*, **874**, L5
- Venhola, A., Peletier, R., Laurikainen, E., et al. 2017, *A&A*, **608**, A142
- Weilbacher, P. M., Duc, P. A., & Fritze-v. Alvensleben, U. 2003, *A&A*, **397**, 545
- Woodley, K. A., Harris, W. E., Beasley, M. A., et al. 2007, *AJ*, **134**, 494
- Zaritsky, D., Donnerstein, R., Dey, A., et al. 2019, *ApJS*, **240**, 1
- Zhu, L., Long, R. J., Mao, S., et al. 2014, *ApJ*, **792**, 59

Appendix A: Potential foreground hosts

The distance estimates of UDG candidates are central to their identification and classification. This is perfectly illustrated by the debate in the literature over the distance to the UDG candidate NGC 1052-DF2. The galaxy was originally assumed to be a satellite of NGC 1052 at a distance of 20 Mpc (van Dokkum et al. 2018b), though it lies in close projection to multiple galaxies: it has a projected separation of 13.7' (~ 80 kpc) from NGC 1052, but also lies in close projection to NGC 1042 (20.8'; ≈ 50 –80 kpc), and is <1 deg from the center of the NGC 988 group (Trujillo et al. 2019), using the coordinates from Kourkchi & Tully (2017). These three host candidates have distances of 20 Mpc, ≈ 8 –13 Mpc, and 15.1 Mpc, respectively, and the UDG would be a typical dwarf at the lower distances. Subsequent independent distance estimates of the galaxy (e.g., spectra, tip of the red giant branch, surface brightness fluctuation, GCLF and planetary nebula luminosity function) have not ended the debate, as they also span the entire range, from ~ 13 Mpc – ~ 22 Mpc (e.g., van Dokkum et al. 2018b; Shen et al. 2021; Blakeslee & Cantiello 2018; Trujillo et al. 2019; Fensch et al. 2019b).

We have assumed throughout the text that the UDGs are satellites of nearby ETGs from the ATLAS^{3D} sample, but this has yet to be proven for the majority of the MATLAS dwarfs. Projection effects can easily confuse which massive galaxy, if any – we cannot rule out the possibility of some fraction of the dwarfs being truly isolated systems –, is the most likely host. In particular, we looked for massive foreground galaxies that could be potential hosts, and which would suggest that the UDGs are closer than we originally assumed.

We constructed a catalog of massive galaxies from the ATLAS^{3D} parent catalog (ETG + LTG galaxies) and supplemented this with galaxies from the NEARGALCAT and the Kourkchi & Tully catalog, after removing duplicate galaxies within a 10'' match radius. We further estimated stellar masses from the available K_s magnitudes, removing any galaxy with $M_*/M_\odot < 10^{9.5}$, the approximate mass of the LMC (van der Marel 2006), as such low mass galaxies are unlikely to host UDGs. Finally, we removed potential host galaxies at distances ≤ 1 Mpc: our UDG candidates do not show the graininess that would be expected if they are within this distance, and this also prevents the nearest massive galaxies (such as M31) from being flagged as a potential host for almost every dwarf in the sample. These restrictions result in a catalog of 2411 potential host galaxies with distances $2.8 \text{ Mpc} < d < 130.2 \text{ Mpc}$ and stellar masses $10^{9.5} < M_*/M_\odot < 10^{11.8}$.

For each UDG in the sample, we then calculated the physical separation between the UDG and each of the 2411 potential hosts, assuming in each instance that the UDG is at the same distance as the potential host galaxy. For this analysis, we kept any potential host with a projected separation < 800 kpc, based on the largest dwarf separation in Cen A (Müller et al. 2018b); this value (800 kpc) is also consistent with the separations of backplash UDG galaxies associated with the galactic-mass host halos simulated in Benavides et al. (2021), although they find that these separations increase to > 3 Mpc in massive groups (see their Figure 7).

The identified potential host galaxies were then plotted versus the distance of the host in Figure A.1, with each subplot corresponding to a single UDG candidate. We note that we also truncated the sample to those galaxies with distances $\lesssim 50$ Mpc in order to focus on foreground hosts. The host galaxies were separated into four mass bins – $< 10^{10}$, 10^{10} – $10^{10.5}$, $10^{10.5}$ – 10^{11} , and

$> 10^{11}$ – and the size of the datapoints increases with increasing mass. We note that the galaxy that we have assumed is the host in this work is marked in pink. Furthermore, the shaded region corresponds to distances at which the effective radius is ≥ 1.5 kpc, meaning that the galaxy would be classified as a UDG anywhere in the shaded region, and dashed red vertical lines mark the independent distance estimates for the three UDGs that have such measurements.

The subplots demonstrate how difficult it is to associate dwarfs/UDGs with a massive host, when no independent distance estimates for the dwarf/UDG exist. Nevertheless, we can make a few broad generalizations. There are a number of systems (19) where the UDG classification appears to be quite secure. This includes subplots where there is a single potential host (e.g., MATLAS-1779), or where there are multiple hosts at roughly similar distances, and the dwarf would be classified as a UDG if it were a satellite of any of these hosts (e.g., MATLAS-42, MATLAS-1855, MATLAS-1996). We still cannot exclude, however, the possibility that these are isolated dwarfs at much lower distances, which would be then be interesting for their isolation rather than their physical diameters.

The remaining systems are more difficult to interpret. There are two systems where all potential foreground hosts (for the remainder of this discussion, ‘foreground hosts’ will be used to indicate any host candidate at distances below the gray shaded ‘UDG region’) that have estimated stellar masses $M_*/M_\odot \leq 10^{10}$; this number jumps to seven if we make a cut at $M_*/M_\odot \leq 10^{10.5}$. Such low mass galaxies are expected to have a very low probability of hosting a UDG, so these dwarfs are likely satellites of more massive, and more distant hosts. If we speculate that the most massive galaxy in each subplot is the most likely potential host, 29/40 of the hosts (59 - 19 = 40; from the paragraph above) lie within the gray shaded ‘UDG region’. It is worth noting, however, that there is one system (MATLAS-262) where *every* potential host has $M_*/M_\odot \leq 10^{10.5}$; the galaxy that we assumed is the host has the highest mass (10.47) of all the potential hosts as well as the smallest physical separation, suggesting that UDGs may be found around some lower mass hosts.

It is readily apparent that some of the assumed distances are suspect, however. As discussed in Section 4, there is confusion between the membership of the NGC 4261 group and the Virgo cluster, which is easily identified by the vertical alignment of points at $d \approx 16$ Mpc (e.g., MATLAS-1246); none of our UDG candidates in the NGC 4261 group would remain UDGs if their distances were revised downward to $d \approx 16$ Mpc. We note that the groups discussed in the main text and Appendix C are not as well defined in these plots as the Virgo cluster. As discussed in Müller et al. (2020), the NGC 5846 group is well defined in velocity space, but independent distance estimates to the most massive members taken from the literature are discrepant by approximately ± 5 Mpc, and this spread can be observed in our plots (e.g., MATLAS-2019); this is likely also a problem for the NGC 4261 group, which additionally suffers from confusion with the foreground Virgo cluster.

Although some of our UDG candidates have several potential foreground hosts – including high mass host candidates and hosts with smaller separations than our tentatively assigned host – it is not always the case that the UDG has a bad distance estimate. MATLAS-1337 has an independent distance estimate based on an HI ALFALFA detection that indicates it is either at a much larger distance than we first assumed, or that it has an inordinately large velocity dispersion ($> 1000 \text{ km s}^{-1}$) for a host at a lower distance.



Fig. A.1. Projected separations in physical units versus the distance to the potential host galaxy for each UDG candidate in the sample. We note that the data has been truncated at separations < 0.8 Mpc and distances $\lesssim 50$ Mpc. The potential hosts have been separated into four mass bins, which is reflected by the size of the data points. The galaxy we have assumed is the host in this work is plotted in *pink*, while the distances at which the dwarf would be considered a UDG are shaded in *gray*. The *dashed red vertical lines* indicate the measured distances, when an estimate is available.

Appendix B: Local environment of UDGs

Spatial maps illustrating the local environment of all UDGs in the MATLAS dwarfs sample are included here, to highlight variations in their environments and complement the discussion of their stacked properties in Section 4. MATLAS pointings that overlap have been combined into a single plot and a buffer of $10'$ around each footprint is included in order to identify any massive galaxies and/or structures that are just outside the MATLAS field of view.

The plots contain:

The ATLAS^{3D} ETG sample: the MATLAS targets were pulled from the ATLAS^{3D} ETG sample, and an ETG is typically centered in (or near the center of) the MegaCam field of view. Plotted as circles, these galaxies are color-coded according to the heliocentric velocities published in Cappellari et al. (2011a). Each galaxy is labeled in the maps.

LTGs in the ATLAS^{3D} parent sample: these galaxies, which meet all of the same selection criteria as the ATLAS^{3D} ETG sample except for morphology, are plotted as diamonds. Like the ETGs, the points are color-coded according to the heliocentric velocities published in Cappellari et al. (2011a) and each galaxy is labeled in the plots.

The MATLAS footprint: The regions imaged as part of the MATLAS survey are shaded pale gray. Where fields overlap, the image size has been adjusted to show all of the contiguous footprints, and the plot bounds were adjusted so that the MATLAS footprint is centered.

The MATLAS dwarf sample: the dwarf galaxies identified by the MATLAS team (Habas et al. 2020; Poulain et al. 2021a) are plotted as small ‘x’ symbols. The distribution of the dwarfs and the highlighted UDG subpopulations can be compared in each map. It should be noted, however, that bright stars and cirrus are not marked; an apparent lack of dwarfs may mean that there are no dwarfs in that region or that they were not visible due to contamination from bright stellar halos or cirrus. The sources of contamination in the MATLAS fields are discussed in Bílek et al. (2020), while Heesters et al. (2021) examines the distribution of dwarfs in the fields and the impact of the stellar halos and cirrus on the dwarf identification.

Ultra diffuse galaxies: the subsample of UDGs identified in this work are plotted as squares. Green squares indicate the UDGs that are not associated with any tidal features, while the turquoise squares indicate UDGs with tidal features – shells, tidal tails, or tidal streams/plumes – and the yellow squares indicate UDGs that are at the end of a tidal tail that is associated with a nearby massive galaxy (see Section 7 for more details).

Groups from Kourkchi & Tully (2017): Kourkchi & Tully created a catalog of groups with recession velocities $< 3500 \text{ km s}^{-1}$ using a galaxy linkage program and expected scaling relations. They published a catalog that includes the luminosity-weighted group center and virial radius for each

group, which we have over-plotted in pale blue. Their galaxy linkage program, however, also links groups of galaxies into larger systems. To focus on the local environment, we plotted only the groups with radii $< 5 \text{ deg}$.

Galaxies from Kourkchi & Tully (2017): Plotting just the galaxies from the ATLAS^{3D} parent sample (ETGs + LTGs) and the MATLAS dwarfs leaves a mass gap ($9 \lesssim \log(M_{\text{stellar}}/M_{\odot}) \lesssim 10$) in the plots, and misses the massive galaxies at distances $d < 10 \text{ Mpc}$ and $d \gtrsim 40 \text{ Mpc}$. To fill in these gaps, we have also plotted the full catalog of galaxies used by Kourkchi & Tully to identify the nearby groups (described above), after removing duplicates from the ATLAS^{3D} sample (260/260 ETGs, 606/611 LTGs) and the MATLAS dwarfs catalog (234/2210 dwarfs). These galaxies are displayed as pentagons. When a distance is available, the pentagons are color-coded according to the velocity, which was calculated assuming only the Hubble flow – and adopting $H_0 = 75 \text{ km s}^{-1}$ as in Kourkchi & Tully (2017) – else they are solid gray.

The color bar on each map spans a unique velocity range. Every massive galaxy (the ATLAS^{3D} ETG + LTG sample and the Kourkchi & Tully catalog) with a measured velocity that falls within the spatial boundaries of the map was taken into account, and the min and max values were rounded down and up, respectively, to the nearest 100 km s^{-1} . Regardless of how wide the spread in velocities is, however, the color bar remains separated into eight colored blocks to better distinguish galaxies in adjoining velocity bins. Velocities for the 325 MATLAS dwarfs with prior distance estimates are not included, to keep the plots cleaner.

While some of the MATLAS fields contain a number of galaxies with a wide spread in velocities ($\Delta v > 2000 \text{ km s}^{-1}$; for example, the field that contains the galaxy pair NGC 5194/NGC 5195, the group including NGC 5169/NGC 5173/NGC 5198, plus a few more distant galaxies) many of the groups are spatially separated from one another. This is not true however for the W Cloud, a.k.a. the NGC 4261 group, which abuts the Virgo cluster. The sharp increase in the number of galaxies in the field is immediately obvious in the relevant subplot below. Properties of this group are uncertain, due to the confusion in separating the group members from the cluster members.

It can be seen in the figures that the UDGs populate a range of environments. As discussed in Section 4, 61% of the UDG sample, as well as two-thirds of the full dwarf sample, falls within the virial radii of one of the Kourkchi & Tully (2017) groups. The dynamical states of the groups is also varied, and UDGs are associated with both dynamically young and dynamically mature groups.

There are also a few potential galaxy pairs/associations that were not identified in the Kourkchi & Tully catalog (e.g., NGC 5506 & NGC 5507) with UDGs nearby, as well as a few relatively isolated hosts (e.g., IC 0560, NGC 5493).

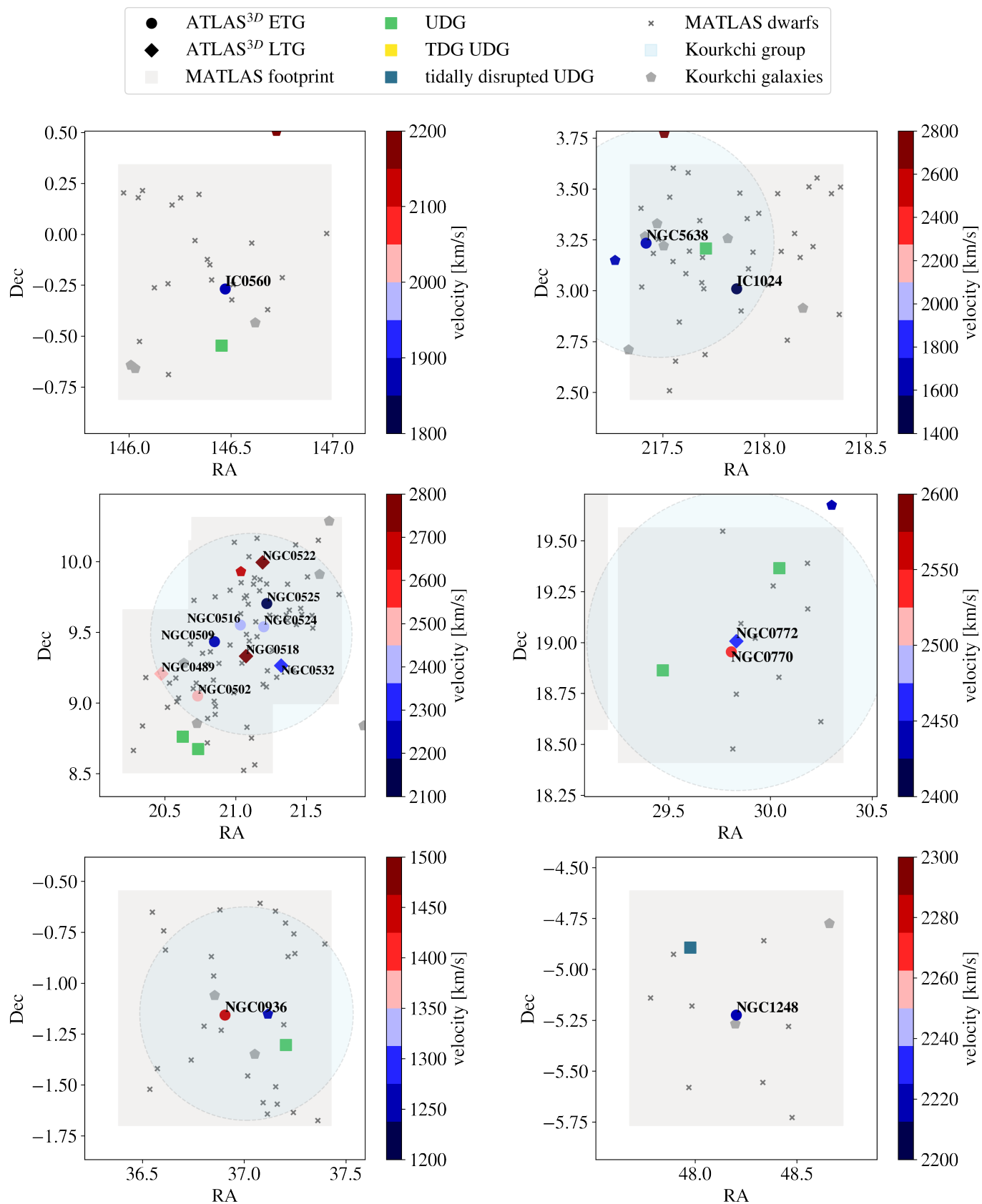


Fig. B.1. Maps of MATLAS fields containing UDGs.

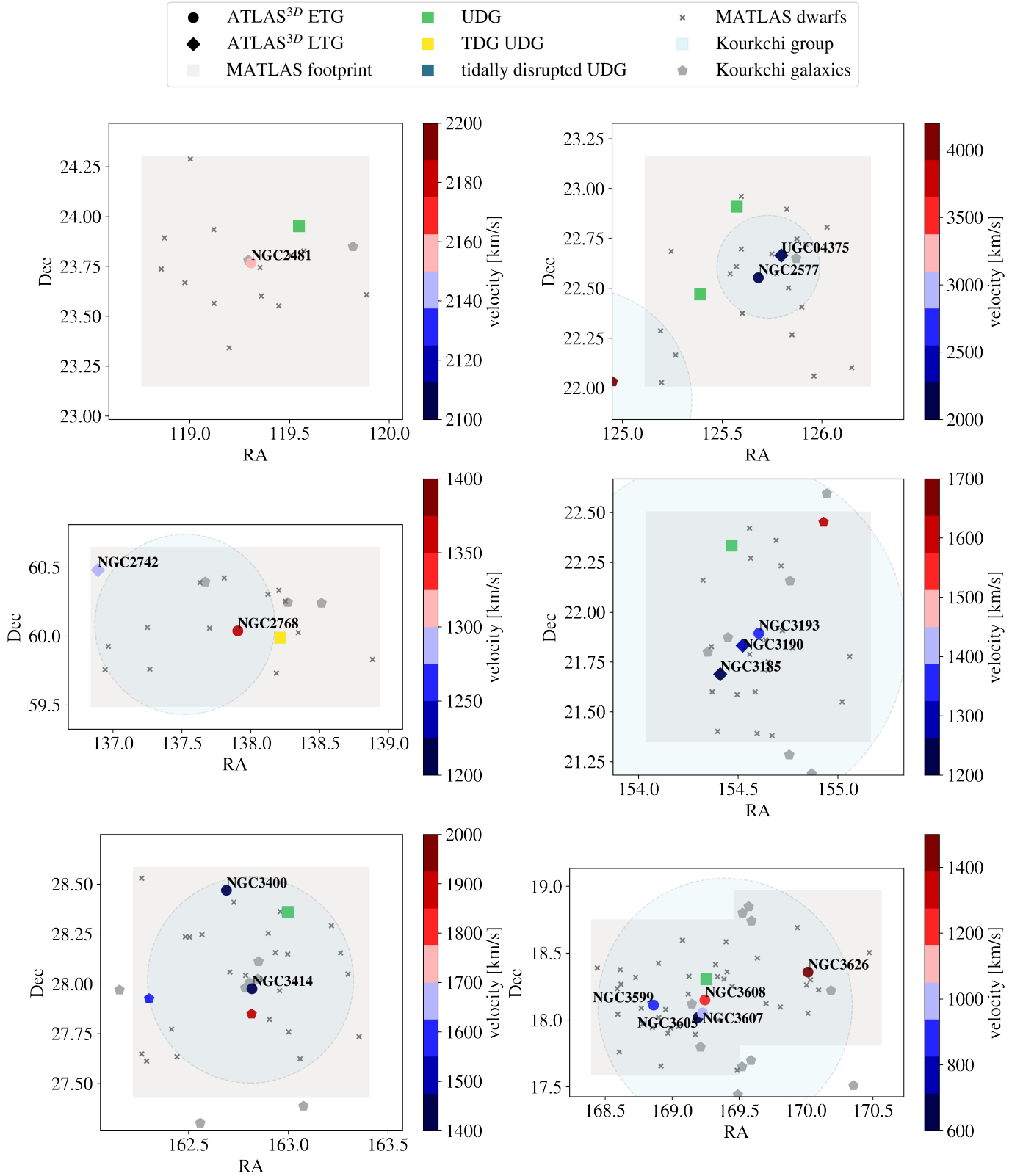


Fig. B.1. (Continued.)

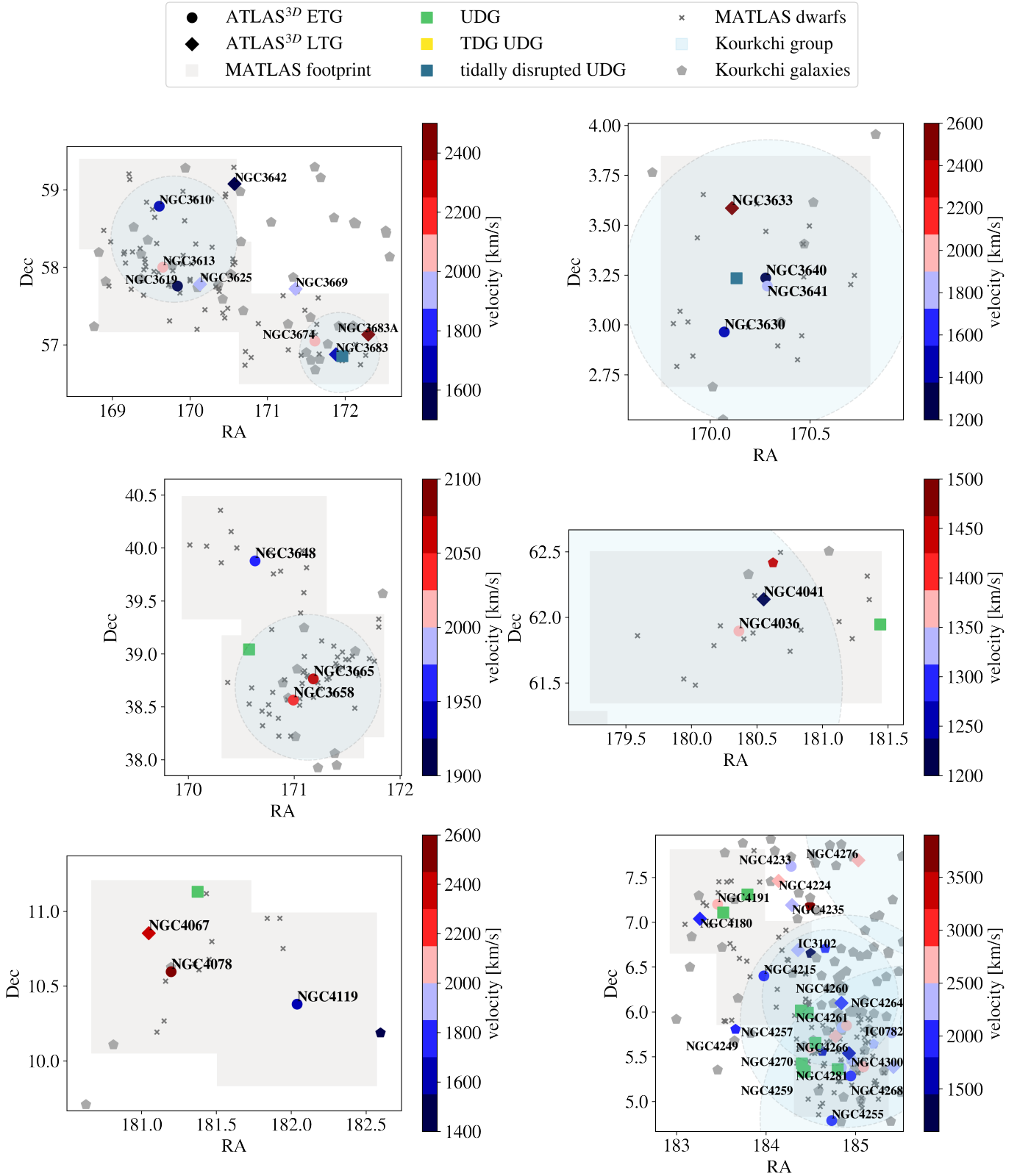


Fig. B.1. (Continued.)

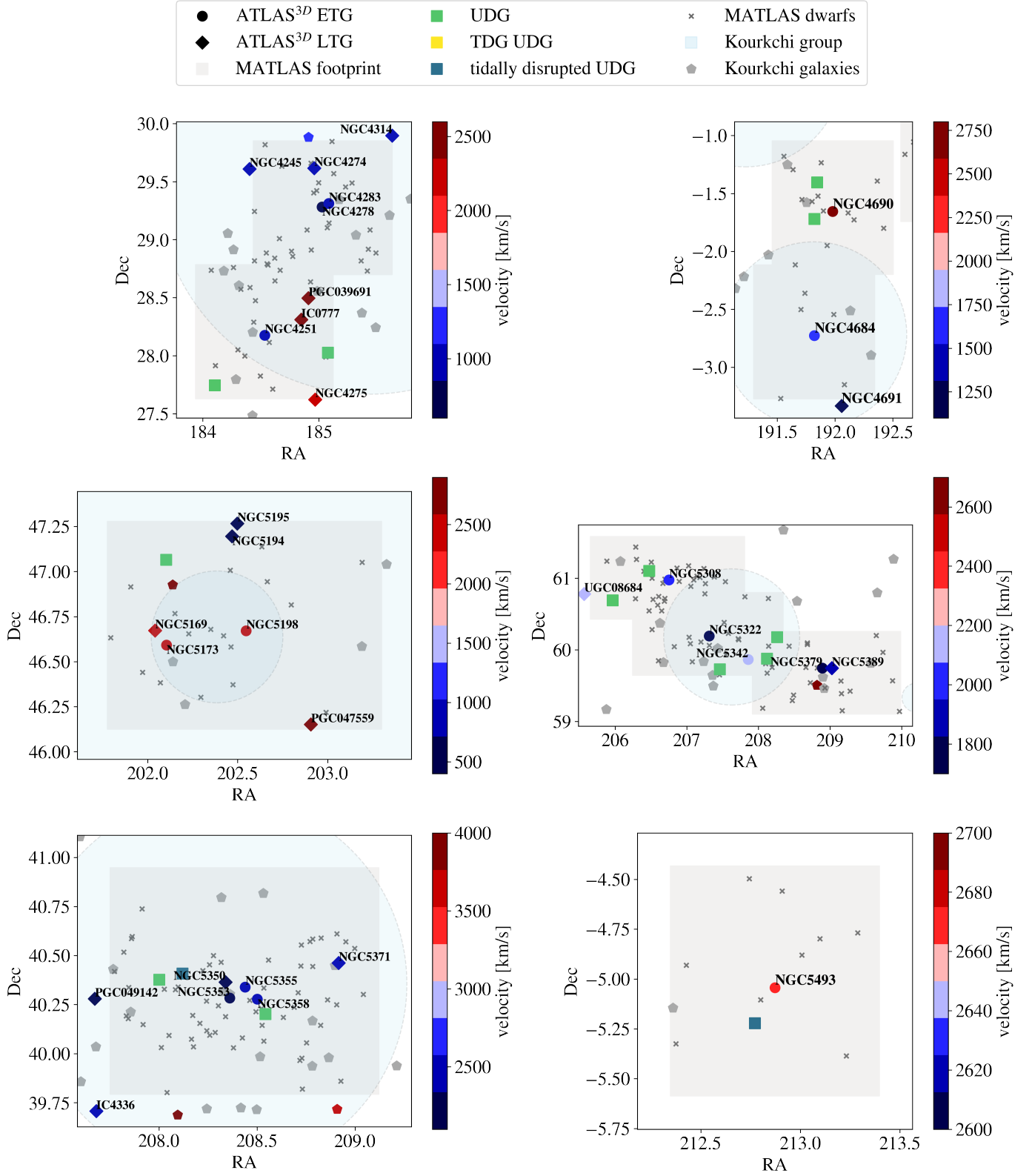


Fig. B.1. (Continued.)

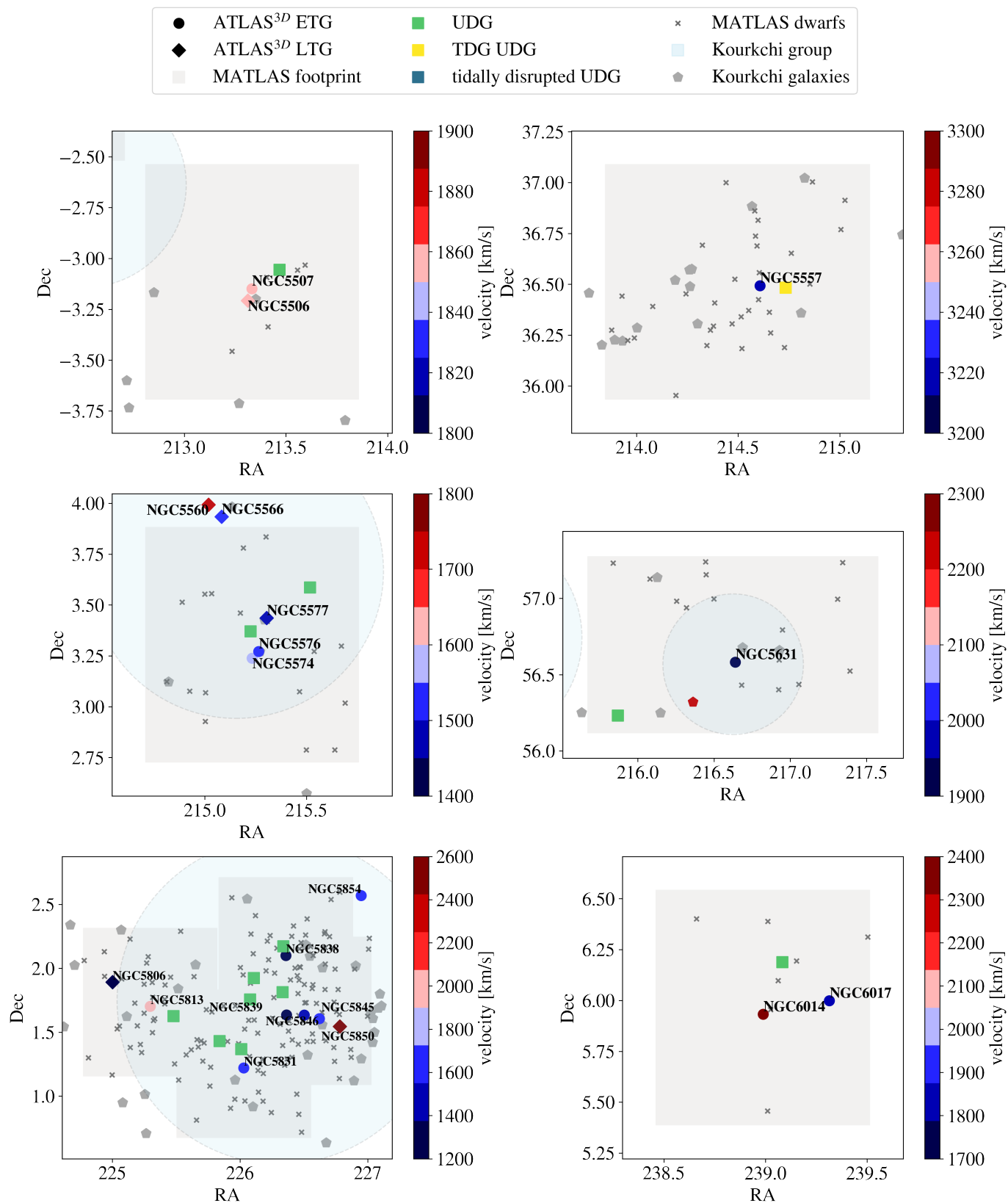


Fig. B.1. (Continued.)

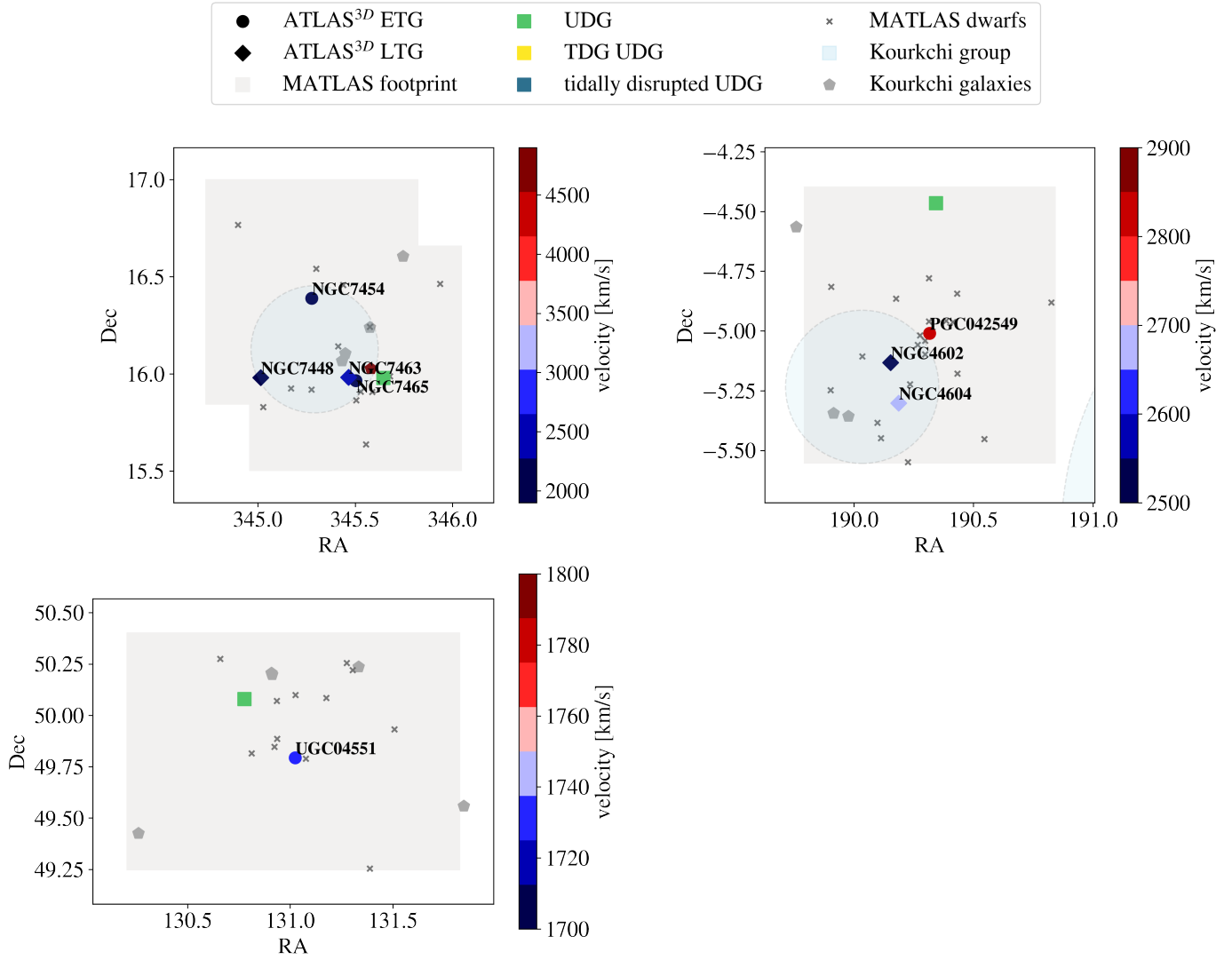


Fig. B.1. (Continued.)

Appendix C: Tables

well as additional derived quantities discussed throughout this work.

The tables in this appendix summarize the photometric properties (morphologies, magnitudes, colors) of the UDG sample as

Table C.1. Photometric properties of the MATLAS UDGs.

| ID | RA | Dec | Morph | Distance | g | $(g-r)_0$ | $(g-i)_0$ | M_g |
|-------------|----------|---------|-------|-----------|----------------|---------------|---------------|-----------------|
| (1) | (2) | (3) | (4) | (Mpc) | (mag) | (mag) | (mag) | (mag) |
| MATLAS-42 | 20.6260 | 8.7614 | dI | 35.9,33.5 | 17.296 ± 0.006 | 0.40 ± 0.02 | 0.55 ± 0.03 | -15.326 ± 0.006 |
| MATLAS-48 | 20.7340 | 8.6737 | dE | 35.9,- | 18.76 ± 0.01 | 0.50 ± 0.01 | 0.72 ± 0.01 | -14.01 ± 0.01 |
| MATLAS-141 | 29.4714 | 18.8628 | dE | 36.7,- | 20.12 ± 0.02 | 0.55 ± 0.03 | 0.90 ± 0.04 | -12.71 ± 0.02 |
| MATLAS-149 | 30.0435 | 19.3647 | dI | 36.7,- | 20.46 ± 0.02 | 0.67 ± 0.03 | 1.01 ± 0.04 | -12.36 ± 0.02 |
| MATLAS-177 | 37.2057 | -1.3041 | dE | 22.4,- | 19.15 ± 0.01 | 0.56 ± 0.02 | 0.83 ± 0.03 | -12.61 ± 0.01 |
| MATLAS-262 | 47.9769 | -4.8931 | dE | 30.4,- | 20.04 ± 0.05 | 0.51 ± 0.05 | - | -12.37 ± 0.05 |
| MATLAS-342 | 119.5476 | 23.9516 | dE | 32.0,- | 18.56 ± 0.02 | - | 0.49 ± 0.06 | -13.97 ± 0.02 |
| MATLAS-365 | 125.3900 | 22.4683 | dE,N | 30.8,- | 19.58 ± 0.10 | 0.72 ± 0.10 | 1.16 ± 0.11 | -12.87 ± 0.10 |
| MATLAS-368 | 125.5731 | 22.9086 | dE,N | 30.8,- | 18.83 ± 0.10 | 0.72 ± 0.02 | 0.82 ± 0.03 | -13.62 ± 0.10 |
| MATLAS-405 | 130.7772 | 50.0784 | dE,N | 28.0,- | 18.87 ± 0.02 | 0.48 ± 0.02 | 0.68 ± 0.02 | -13.37 ± 0.02 |
| MATLAS-478 | 138.2168 | 59.9870 | dE,N | 21.8,- | 17.486 ± 0.006 | 0.526 ± 0.007 | 0.85 ± 0.01 | -14.207 ± 0.006 |
| MATLAS-585 | 146.4547 | -0.5469 | dE | 27.2,- | 18.789 ± 0.005 | 0.36 ± 0.02 | - | -13.384 ± 0.005 |
| MATLAS-658 | 154.4670 | 22.3337 | dE | 33.1,- | 20.63 ± 0.17 | - | - | -11.97 ± 0.17 |
| MATLAS-799 | 162.9980 | 28.3601 | dE | 24.5,- | 17.28 ± 0.006 | 0.577 ± 0.007 | - | -14.669 ± 0.006 |
| MATLAS-898 | 169.2570 | 18.3027 | dE | 19.8,- | 17.94 ± 0.02 | 0.35 ± 0.05 | 0.61 ± 0.05 | -13.55 ± 0.02 |
| MATLAS-951 | 170.1326 | 3.2332 | dE,N | 26.3,- | 18.023 ± 0.006 | 0.679 ± 0.007 | 1.052 ± 0.009 | -14.076 ± 0.006 |
| MATLAS-984 | 170.5741 | 39.0399 | dE | 33.1,- | 19.26 ± 0.02 | 0.39 ± 0.02 | 0.68 ± 0.03 | -13.34 ± 0.02 |
| MATLAS-1059 | 171.9652 | 56.8550 | dE,N | 33.4,- | 18.099 ± 0.006 | 0.488 ± 0.008 | - | -14.520 ± 0.006 |
| MATLAS-1174 | 181.3757 | 11.1305 | dE | 38.1,- | 19.73 ± 0.02 | 0.16 ± 0.06 | - | -13.17 ± 0.02 |
| MATLAS-1177 | 181.4412 | 61.9456 | dE,N | 24.6,- | 18.357 ± 0.005 | 0.55 ± 0.01 | - | -13.597 ± 0.005 |
| MATLAS-1205 | 183.5229 | 7.1086 | dE,N | 39.2,- | 19.500 ± 0.005 | 0.48 ± 0.01 | - | -13.467 ± 0.005 |
| MATLAS-1216 | 183.7925 | 7.3112 | dE,N | 39.2,- | 20.02 ± 0.03 | 0.52 ± 0.04 | - | -12.95 ± 0.03 |
| MATLAS-1225 | 184.1047 | 27.7437 | dE | 19.1,- | 18.50 ± 0.02 | - | - | -12.90 ± 0.01 |
| MATLAS-1245 | 184.3903 | 6.0166 | dE | 31.5,- | 19.44 ± 0.02 | 0.29 ± 0.06 | - | -13.05 ± 0.02 |
| MATLAS-1246 | 184.4013 | 5.4247 | dE | 37.2,- | 18.04 ± 0.01 | 0.61 ± 0.01 | 0.86 ± 0.01 | -14.82 ± 0.01 |
| MATLAS-1248 | 184.4155 | 5.3419 | dE | 37.2,- | 17.56 ± 0.005 | 0.64 ± 0.01 | 0.89 ± 0.02 | -15.292 ± 0.005 |
| MATLAS-1249 | 184.4336 | 5.3309 | dE | 37.2,- | 19.57 ± 0.07 | 0.79 ± 0.09 | 1.17 ± 0.11 | -13.29 ± 0.07 |
| MATLAS-1262 | 184.4664 | 5.9891 | dE,N | 31.5,- | 18.69 ± 0.02 | 0.55 ± 0.03 | - | -13.81 ± 0.02 |
| MATLAS-1274 | 184.5520 | 5.6525 | dE | 37.2,- | 17.586 ± 0.006 | 0.517 ± 0.009 | 0.70 ± 0.01 | -15.276 ± 0.006 |
| MATLAS-1302 | 184.8020 | 5.3615 | dE | 37.2,- | 20.82 ± 0.03 | 0.55 ± 0.04 | 0.82 ± 0.05 | -12.03 ± 0.03 |
| MATLAS-1337 | 185.0780 | 28.0257 | dI,N | 19.1,35.9 | 18.514 ± 0.006 | - | - | -14.264 ± 0.006 |
| MATLAS-1413 | 190.3429 | -4.4653 | dE | 40.7,- | 19.39 ± 0.02 | 0.74 ± 0.05 | - | -13.65 ± 0.02 |
| MATLAS-1493 | 191.8227 | -1.7204 | dE,N | 40.2,- | 19.88 ± 0.02 | 0.51 ± 0.02 | - | -13.14 ± 0.02 |
| MATLAS-1494 | 191.8468 | -1.4045 | dE | 40.2,- | 18.833 ± 0.009 | 0.50 ± 0.01 | - | -14.188 ± 0.009 |
| MATLAS-1534 | 202.1029 | 47.0652 | dE | 39.6,- | 20.27 ± 0.02 | 0.43 ± 0.04 | - | -12.72 ± 0.02 |
| MATLAS-1550 | 205.9650 | 60.6890 | dE | 31.5,- | 19.52 ± 0.01 | 0.49 ± 0.02 | - | -12.97 ± 0.01 |
| MATLAS-1558 | 206.4767 | 61.0976 | dE,N | 31.5,- | 19.51 ± 0.02 | 0.65 ± 0.02 | - | -12.98 ± 0.02 |
| MATLAS-1589 | 207.4632 | 59.7278 | dE | 30.3,- | 19.95 ± 0.02 | 0.47 ± 0.02 | - | -12.46 ± 0.02 |
| MATLAS-1606 | 208.0022 | 40.3767 | dE,N | 37.1,- | 18.453 ± 0.002 | - | - | -14.394 ± 0.002 |
| MATLAS-1615 | 208.1200 | 40.4081 | dE,N | 37.1,- | 18.11 ± 0.01 | 0.60 ± 0.01 | 0.89 ± 0.01 | -14.74 ± 0.01 |
| MATLAS-1616 | 208.1220 | 59.8762 | dE,N | 30.0,- | 18.68 ± 0.05 | 0.58 ± 0.05 | - | -13.71 ± 0.02 |
| MATLAS-1630 | 208.2604 | 60.1730 | dE | 30.3,- | 19.23 ± 0.02 | 0.78 ± 0.03 | 1.14 ± 0.03 | -13.17 ± 0.02 |
| MATLAS-1647 | 208.5436 | 40.2012 | dE | 37.1,- | 20.75 ± 0.02 | 0.81 ± 0.02 | 1.08 ± 0.03 | -12.10 ± 0.02 |
| MATLAS-1779 | 212.7722 | -5.2221 | dE,N | 38.8,- | 19.27 ± 0.02 | 0.49 ± 0.12 | - | -13.67 ± 0.02 |
| MATLAS-1794 | 213.4693 | -3.0559 | dE | 28.5,- | 19.02 ± 0.02 | - | - | -13.25 ± 0.02 |
| MATLAS-1824 | 214.7337 | 36.4832 | dE | 38.8,46.3 | 18.44 ± 0.01 | 0.06 ± 0.02 | 0.07 ± 0.03 | -14.89 ± 0.01 |
| MATLAS-1847 | 215.2256 | 3.3710 | dE | 23.2,- | 18.77 ± 0.05 | 0.56 ± 0.05 | - | -13.06 ± 0.04 |
| MATLAS-1855 | 215.5181 | 3.5866 | dE,N | 23.2,- | 18.67 ± 0.05 | 0.36 ± 0.05 | - | -13.16 ± 0.05 |
| MATLAS-1865 | 215.8694 | 56.2322 | dE | 27.0,- | 18.53 ± 0.01 | 0.22 ± 0.01 | 0.31 ± 0.02 | -13.628 ± 0.008 |
| MATLAS-1907 | 217.7121 | 3.2066 | dE | 24.2,- | 18.150 ± 0.004 | 0.492 ± 0.005 | - | -13.769 ± 0.004 |
| MATLAS-1957 | 225.4779 | 1.6258 | dE,N | 31.3,- | 18.46 ± 0.10 | - | - | -14.01 ± 0.02 |
| MATLAS-1975 | 225.8389 | 1.4309 | dE,N | 26.4,- | 19.23 ± 0.07 | 0.43 ± 0.17 | - | -12.88 ± 0.07 |
| MATLAS-1985 | 226.0105 | 1.3671 | dE | 26.4,- | 18.850 ± 0.006 | - | - | -13.258 ± 0.006 |

Table C.1. continued.

| ID | RA | Dec | Morph | Distance | g | $(g-r)_0$ | $(g-i)_0$ | M_g |
|-------------|----------|---------|-------|-----------|----------------|--------------|--------------|-----------------|
| (1) | (2) | (3) | (4) | (Mpc) | (mag) | (mag) | (mag) | (mag) |
| | | | | (5) | (6) | (7) | (8) | (9) |
| MATLAS-1991 | 226.0792 | 1.7555 | dE | 25.2,- | 18.061 ± 0.004 | 0.59 ± 0.02 | 0.87 ± 0.03 | -13.946 ± 0.004 |
| MATLAS-1996 | 226.1090 | 1.9246 | dE | 21.8,- | 19.95 ± 0.13 | - | - | -11.75 ± 0.13 |
| MATLAS-2019 | 226.3340 | 1.8127 | dE | 25.2,20.0 | 17.79 ± 0.01 | 0.59 ± 0.02 | 0.85 ± 0.02 | -13.74 ± 0.01 |
| MATLAS-2021 | 226.3400 | 2.1722 | dE | 21.8,- | 19.35 ± 0.08 | -0.03 ± 0.12 | -0.19 ± 0.34 | -12.34 ± 0.08 |
| MATLAS-2103 | 239.0837 | 6.1882 | dE | 35.8,- | 18.037 ± 0.006 | - | - | -14.733 ± 0.006 |
| MATLAS-2184 | 345.6448 | 15.9791 | dE | 29.3,- | 19.39 ± 0.05 | 0.12 ± 0.05 | 0.18 ± 0.06 | -12.95 ± 0.05 |

Notes. This table (including previous page) is available at the CDS. Columns meanings: (1) UDG ID; (2) and (3) Right ascension and declination; (4) Morphology; (5) Assumed host ETG distance, dwarf distance; (6) Apparent magnitude in the g -band; (7) $g-r$ color corrected for Galactic extinction; (8) $g-i$ color corrected for Galactic extinction; (9) Absolute magnitude in the g -band computed using the UDG distance when available, otherwise the assumed host ETG distance is used.

Table C.2. Additional properties of the MATLAS UDGs.

| ID | $\mu_{0,g}$ | $\langle \mu_{e,g} \rangle$ | $R_{e,g}$ | $R_{e,g}$ | $\log(M_*/M_\odot)$ | M_{halo}/M_* |
|-------------|----------------------------|-----------------------------|---------------|---------------|---------------------|-------------------------------------------|
| (1) | (mag/arcsec ²) | (mag/arcsec ²) | (arcsec) | (kpc) | (6) | (7) |
| | (2) | (3) | (4) | (5) | | |
| MATLAS-42 | 24.39 ± 0.02 | 25.17 ± 0.02 | 21.19 ± 0.13 | 3.46 ± 0.02 | 8.32 ± 0.16 | - |
| MATLAS-48 | 24.38 ± 0.04 | 25.17 ± 0.04 | 10.75 ± 0.12 | 1.89 ± 0.02 | 7.95 ± 0.17 | - |
| MATLAS-141 | 25.22 ± 0.08 | 26.00 ± 0.08 | 8.48 ± 0.22 | 1.52 ± 0.04 | 7.51 ± 0.14 | - |
| MATLAS-149 | 25.97 ± 0.09 | 26.75 ± 0.09 | 10.24 ± 0.31 | 1.84 ± 0.06 | 7.55 ± 0.14 | - |
| MATLAS-177 | 25.36 ± 0.05 | 26.15 ± 0.05 | 14.17 ± 0.22 | 1.55 ± 0.02 | 7.49 ± 0.15 | 158.5 ^{+155.2} _{-88.4} |
| MATLAS-262 | 26.84 ± 0.17 | 27.63 ± 0.17 | 18.56 ± 1.04 | 2.75 ± 0.16 | 7.32 ± 0.13 | - |
| MATLAS-342 | 24.02 ± 0.07 | 24.80 ± 0.07 | 10.02 ± 0.22 | 1.57 ± 0.04 | - | - |
| MATLAS-365 | 25.05 ± 0.30 | 25.84 ± 0.30 | 10.08 ± 0.88 | 1.52 ± 0.13 | 7.83 ± 0.06 | - |
| MATLAS-368 | 24.50 ± 0.14 | 25.28 ± 0.14 | 11.03 ± 0.22 | 1.66 ± 0.03 | 8.13 ± 0.15 | 55.6 ^{+54.5} _{-31.1} |
| MATLAS-405 | 25.33 ± 0.05 | 26.11 ± 0.05 | 15.86 ± 0.27 | 2.17 ± 0.04 | 7.66 ± 0.16 | - |
| MATLAS-478 | 24.55 ± 0.02 | 25.33 ± 0.02 | 20.94 ± 0.13 | 2.22 ± 0.01 | 8.07 ± 0.17 | - |
| MATLAS-585 | 24.59 ± 0.02 | 25.37 ± 0.02 | 11.68 ± 0.08 | 1.55 ± 0.01 | 7.50 ± 0.15 | - |
| MATLAS-658 | 25.93 ± 0.67 | 26.71 ± 0.67 | 9.28 ± 1.93 | 1.50 ± 0.31 | - | - |
| MATLAS-799 | 23.98 ± 0.02 | 24.76 ± 0.02 | 17.74 ± 0.10 | 2.12 ± 0.01 | 8.33 ± 0.17 | - |
| MATLAS-898 | 24.54 ± 0.06 | 25.32 ± 0.06 | 16.92 ± 0.34 | 1.63 ± 0.03 | 7.54 ± 0.13 | 325.6 ^{+314.7} _{-174.3} |
| MATLAS-951 | 25.23 ± 0.02 | 26.02 ± 0.02 | 22.39 ± 0.18 | 2.87 ± 0.23 | 8.25 ± 0.17 | 38.9 ^{+38.4} _{-22.2} |
| MATLAS-984 | 24.59 ± 0.06 | 25.37 ± 0.06 | 9.40 ± 0.18 | 1.52 ± 0.03 | 7.52 ± 0.16 | - |
| MATLAS-1059 | 24.30 ± 0.02 | 25.08 ± 0.02 | 14.05 ± 0.09 | 2.29 ± 0.02 | 8.14 ± 0.17 | - |
| MATLAS-1174 | 25.66 ± 0.08 | 26.44 ± 0.08 | 12.38 ± 0.33 | 2.31 ± 0.06 | 7.10 ± 0.12 | - |
| MATLAS-1177 | 24.42 ± 0.02 | 25.21 ± 0.02 | 13.22 ± 0.09 | 1.59 ± 0.01 | 7.86 ± 0.16 | 208.3 ^{+205.2} _{-118.3} |
| MATLAS-1205 | 24.817 ± 0.006 | 25.599 ± 0.006 | 9.362 ± 0.007 | 1.795 ± 0.001 | 7.71 ± 0.16 | - |
| MATLAS-1216 | 25.94 ± 0.10 | 26.72 ± 0.10 | 12.35 ± 0.38 | 2.37 ± 0.07 | 7.56 ± 0.14 | - |
| MATLAS-1225 | 25.29 ± 0.05 | 26.07 ± 0.05 | 18.43 ± 0.27 | 1.71 ± 0.03 | - | - |
| MATLAS-1245 | 25.74 ± 0.08 | 26.53 ± 0.08 | 14.75 ± 0.39 | 2.27 ± 0.06 | 7.26 ± 0.10 | - |
| MATLAS-1246 | 24.22 ± 0.03 | 25.01 ± 0.03 | 13.98 ± 0.13 | 2.54 ± 0.02 | 8.45 ± 0.17 | 32.9 ^{+32.4} _{-18.7} |
| MATLAS-1248 | 23.95 ± 0.02 | 24.73 ± 0.02 | 15.35 ± 0.09 | 2.79 ± 0.02 | 8.68 ± 0.17 | 22.4 ^{+22.1} _{-12.8} |
| MATLAS-1249 | 25.21 ± 0.21 | 26.00 ± 0.21 | 10.91 ± 0.70 | 1.98 ± 0.13 | 8.10 ± 0.06 | - |
| MATLAS-1262 | 24.46 ± 0.07 | 25.24 ± 0.07 | 11.55 ± 0.24 | 1.78 ± 0.04 | 7.95 ± 0.14 | 390.9 ^{+380.8} _{-214.5} |
| MATLAS-1274 | 23.96 ± 0.02 | 24.75 ± 0.02 | 15.26 ± 0.09 | 2.78 ± 0.02 | 8.48 ± 0.17 | - |

Table C.2. continued.

| ID | $\mu_{0,g}$ (mag/arcsec ²) | $\langle\mu_{e,g}\rangle$ (mag/arcsec ²) | $R_{e,g}$ (arcsec) | $R_{e,g}$ (kpc) | $\log(M_*/M_\odot)$ | M_{halo}/M_* |
|-------------|-------------------------------------------|---------------------------------------------------------|-----------------------|--------------------|---------------------|----------------------------------------------|
| (1) | (2) | (3) | (4) | (5) | (6) | (7) |
| MATLAS-1302 | 25.90 ± 0.13 | 26.68 ± 0.13 | 8.36 ± 0.35 | 1.52 ± 0.06 | 7.24 ± 0.13 | – |
| MATLAS-1337 | 24.20 ± 0.03 | 24.98 ± 0.03 | 11.08 ± 0.10 | 1.95 ± 0.02 | – | – |
| MATLAS-1413 | 25.94 ± 0.07 | 26.72 ± 0.07 | 16.47 ± 0.40 | 3.28 ± 0.08 | 8.17 ± 0.10 | – |
| MATLAS-1493 | 24.88 ± 0.06 | 25.67 ± 0.06 | 8.12 ± 0.16 | 1.60 ± 0.03 | 7.62 ± 0.16 | – |
| MATLAS-1494 | 24.88 ± 0.03 | 25.66 ± 0.03 | 13.09 ± 0.14 | 2.57 ± 0.03 | 8.03 ± 0.17 | – |
| MATLAS-1534 | 25.21 ± 0.06 | 26.00 ± 0.06 | 7.88 ± 0.16 | 1.53 ± 0.03 | 7.34 ± 0.13 | – |
| MATLAS-1550 | 25.09 ± 0.04 | 25.87 ± 0.04 | 10.50 ± 0.15 | 1.62 ± 0.02 | 7.53 ± 0.16 | – |
| MATLAS-1558 | 25.83 ± 0.05 | 26.61 ± 0.05 | 14.84 ± 0.25 | 2.28 ± 0.04 | 7.77 ± 0.15 | 250.3 ^{+245.1} _{–139.6} |
| MATLAS-1589 | 25.73 ± 0.06 | 26.51 ± 0.06 | 11.61 ± 0.24 | 1.72 ± 0.04 | 7.29 ± 0.15 | – |
| MATLAS-1606 | 24.435 ± 0.003 | 25.217 ± 0.003 | 12.713 ± 0.008 | 2.306 ± 0.002 | – | – |
| MATLAS-1615 | 24.58 ± 0.04 | 25.36 ± 0.04 | 15.90 ± 0.17 | 2.88 ± 0.03 | 8.39 ± 0.17 | 167.4 ^{+165.0} _{–95.3} |
| MATLAS-1616 | 25.12 ± 0.08 | 25.90 ± 0.08 | 15.67 ± 0.22 | 2.30 ± 0.03 | 7.95 ± 0.16 | 160.1 ^{+137.3} _{–90.3} |
| MATLAS-1630 | 25.18 ± 0.08 | 25.97 ± 0.08 | 12.52 ± 0.31 | 1.85 ± 0.05 | 8.04 ± 0.15 | – |
| MATLAS-1647 | 25.81 ± 0.07 | 26.59 ± 0.07 | 8.30 ± 0.21 | 1.51 ± 0.04 | 7.65 ± 0.15 | – |
| MATLAS-1779 | 25.65 ± 0.06 | 26.44 ± 0.06 | 15.30 ± 0.22 | 2.90 ± 0.04 | 7.80 ± 0.02 | 912.3 ^{+852.0} _{–432.4} |
| MATLAS-1794 | 24.95 ± 0.07 | 25.73 ± 0.07 | 12.39 ± 0.29 | 1.72 ± 0.04 | – | – |
| MATLAS-1824 | 24.36 ± 0.04 | 25.14 ± 0.04 | 12.37 ± 0.14 | 2.81 ± 0.03 | 7.65 ± 0.17 | – |
| MATLAS-1847 | 25.40 ± 0.11 | 26.18 ± 0.11 | 17.12 ± 0.49 | 1.94 ± 0.06 | 7.66 ± 0.12 | 352.0 ^{+339.7} _{–187.5} |
| MATLAS-1855 | 24.84 ± 0.13 | 25.63 ± 0.13 | 13.90 ± 0.48 | 1.57 ± 0.05 | 7.41 ± 0.13 | 556.2 ^{+537.5} _{–297.5} |
| MATLAS-1865 | 24.35 ± 0.03 | 25.13 ± 0.03 | 11.80 ± 0.13 | 1.55 ± 0.02 | 7.38 ± 0.18 | 1897.1 ^{+1879.3} _{–1095.8} |
| MATLAS-1907 | 24.21 ± 0.02 | 24.99 ± 0.02 | 13.15 ± 0.07 | 1.552 ± 0.009 | 7.85 ± 0.18 | – |
| MATLAS-1957 | 24.07 ± 0.14 | 24.85 ± 0.14 | 10.67 ± 0.22 | 1.63 ± 0.03 | – | – |
| MATLAS-1975 | 25.18 ± 0.24 | 25.96 ± 0.24 | 12.54 ± 0.91 | 1.61 ± 0.12 | 7.40 ± 0.04 | 316.5 ^{+297.0} _{–152.8} |
| MATLAS-1985 | 25.11 ± 0.03 | 25.90 ± 0.03 | 14.48 ± 0.13 | 1.87 ± 0.02 | – | – |
| MATLAS-1991 | 24.01 ± 0.02 | 24.79 ± 0.02 | 12.52 ± 0.07 | 1.538 ± 0.009 | 8.06 ± 0.15 | 140.8 ^{+137.9} _{–78.7} |
| MATLAS-1996 | 26.27 ± 0.19 | 27.05 ± 0.19 | 14.87 ± 0.45 | 1.58 ± 0.05 | – | – |
| MATLAS-2019 | 24.42 ± 0.04 | 25.21 ± 0.04 | 17.16 ± 0.21 | 1.69 ± 0.02 | 7.99 ± 0.15 | 930.7 ^{+911.8} _{–519.9} |
| MATLAS-2021 | 26.06 ± 0.19 | 26.84 ± 0.19 | 17.79 ± 0.91 | 1.89 ± 0.10 | 6.49 ± 0.04 | 727.6 ^{+682.7} _{–351.0} |
| MATLAS-2103 | 24.27 ± 0.02 | 25.05 ± 0.02 | 14.25 ± 0.10 | 2.49 ± 0.02 | – | – |
| MATLAS-2184 | 25.17 ± 0.16 | 25.96 ± 0.16 | 11.61 ± 0.54 | 1.66 ± 0.08 | 6.96 ± 0.13 | – |

Notes. This table (including previous page) is available at the CDS. Columns meanings: (1) UDG ID; (2) Central surface brightness in the g -band; (3) Average surface brightness within R_e in the g -band; (4) Effective radius in arcsec in the g -band; (5) Effective radius in kpc in the g -band computed using the UDG distance when available, otherwise the assumed host distance is used; (6) Stellar mass computed based on the stellar mass-to-light ratios from [Bell et al. \(2003\)](#) and the derived $(g-r)_0$ color using the formula $\log(M_*/M_\odot) = -0.306 + 1.097(g-r)_0 - 0.4(M_r - 4.77)$; (7) Halo-to-stellar mass ratio computed based on the mass ratio from [Harris et al. \(2017\)](#) and the derived GC count using the formula $M_{halo} = M_{GC,tot}/2.9 \times 10^{-5}$.